Aus der Klinik für Psychiatrie und Psychotherapie
der Medizinischen Fakultät Charité – Universitätsmedizin Berlin

DISSERTATION

Pericytes in Alzheimer's Disease: A Morphometric Analysis

zur Erlangung des akademischen Grades
Doctor medicinae (Dr. med.)

vorgelegt der Medizinischen Fakultät
Charité – Universitätsmedizin Berlin

von

Lasse Brandt

aus Kiel, Deutschland

Datum der Promotion: 04.03.2022

Preface

Preliminary findings of this dissertation have been presented as a poster at the XI European Meeting on Glial Cells in Health and Disease, Berlin, July 3-6, 2013:

Brandt L*, Fernández-Klett F*, Harris LW, Bahn S, Priller J. Pericytes are preserved in Alzheimer's disease. *Glia* 2013; **61**: 65–6. doi:10.1002/glia.22530. *Contributed equally as co–first authors.

The poster includes preliminary parts of the abstract, introduction, methods, results, and discussion from this dissertation.

Findings of this dissertation have been published as an article:

Fernández-Klett F*, Brandt L*, Fernández Zapata C, Abuelnor B, Middeldorp J, Sluijs JA, Curtis M, Faull R, Harris LW, Bahn S, Hol EM, Priller J. Denser brain capillary network with preserved pericytes in Alzheimer's disease. *Brain Pathol* 2020; **30**: 1071–86. doi:10.1111/bpa.12897. *Contributed equally as co–first authors.

The article includes parts of the abstract, introduction, methods, results, and discussion from this dissertation.

Table of contents

Index of figures and tables

Figures

Tables

Abbreviations

ABC	Avidin biotin complex
AD	Alzheimer's disease
APOE	Apolipoprotein E
APP	Amyloid precursor protein
ASF	Area sampling fraction
Aβ	Amyloid beta
BBB	Blood-brain barrier
CATCH	Critically attained threshold of cerebral hypoperfusion
CBF	Cerebral blood flow
CERAD	Consortium to Establish a Registry for Alzheimer's Disease
CNS	Central nervous system
HSF	Height sampling fraction
MRI	Magnetic resonance imaging
NA	Numerical aperture
NDS	Normal donkey serum
NFT	Neurofibrillary tangle
NHS	Normal horse serum
NIA-RI	National Institute on Aging and Reagan Institute
PDGF-BB	Platelet-derived growth factor-BB
PDGFRβ	Platelet-derived growth factor receptor beta
PET	Positron emission tomography
PMT	Post-mortem time
ROI	Region of interest
SRS	Systematic random sampling
SSF	Section sampling fraction
TBS	Tris-buffered saline
VEGF	Vascular endothelial growth factor

Abstract

Pericytes extend within the basement membranes of the microvasculature, maintain the blood-brain barrier integrity, and contribute to neurovascular regulation. Studies have suggested that pericyte dysfunction and loss play important roles in impaired blood-brain barriers and neurovascular dysregulation in Alzheimer's disease (AD).

The primary objective of this study was to investigate if pericyte loss occurs in AD pathology. We employed morphometric techniques and investigated the vasculature in the grey matter of the middle frontal gyrus. Samples were obtained post-mortem from 16 AD cases and 16 control cases without a history of dementia. Markers of pericytes (platelet-derived growth factor receptor beta), vessels (laminin), cell proliferation (Ki67), and amyloid beta were immunostained. The analyses of pericyte density (pericytes per tissue volume), pericyte linear density (pericytes per capillary length), and vessel density (vessel length per tissue volume) were performed with the stereological methods optical fractionator and spaceballs. We measured pericyte coverage (percentage of capillary area covered by pericytes) with an image threshold technique and amyloid beta (percentage of tissue area covered by amyloid beta) with the stereological area fraction fractionator tool.

There were no significant differences in pericyte linear density (control vs. AD; mean ± SD; 8.3 ± 0.7 vs. 8.5 ± 1 cells / mm capillary; $p = 0.4635$) or coverage (control vs. AD; median 75.6 vs. 75.8 % area; $p = 0.7804$) between control and AD cases. Compared to controls, AD subjects were characterized by a 24% increase in capillary density (control vs. AD; mean ± SD; 291 ± 39 vs. 361 ± 48 mm / mm^3; $p < 0.0001$), paralleled by a 28% increase in pericyte density (control vs. AD; mean ± SD; 2412 ± 376 vs. 3081 ± 584 cells / mm^3; $p = 0.0006$). The increase in vessel density was limited to capillaries and did not include other parenchymal vessels. Capillary density showed a strong positive correlation with total amyloid beta (control and AD; $r_s = 0.6419$, $p < 0.0001$). Proliferating pericytes and endothelial cells were rare in both control and AD.

Our results indicate that AD pathology in the middle frontal cortex is characterized by an increase in the density of capillaries, which maintain a morphometrically normal pericyte population. This suggests that the neurovascular and blood-brain barrier abnormalities found in AD pathology may not be the consequence of pericyte loss.

Abstract (deutsche Übersetzung)

Perizyten befinden sich innerhalb der Basalmembran der Mikrovaskulatur und tragen zur Integrität der Blut-Hirn-Schranke und neurovaskulären Regulation bei. Studien haben nahegelegt, dass Perizytendysfunktion und -verlust eine wichtige Rolle bei gestörten Blut-Hirn-Schranken und neurovaskulärer Dysregulation in der Alzheimer-Pathologie spielen.

Primäres Ziel dieser Studie war, zu untersuchen, ob Perizytenverlust in der Alzheimer-Pathologie auftritt. Dazu setzten wir morphometrische Techniken ein und untersuchten die Gefäße in der Grauen Substanz des mittleren frontalen Gyrus. Post-mortem-Gewebeproben stammten von 16 Subjekten mit Alzheimer-Krankheit (AK) und 16 Kontroll-Subjekten ohne demenzieller Vorerkrankung. Marker von Perizyten (Platelet-Derived Growth Factor Receptor Beta), Gefäßen (Laminin), Zell-Proliferation (Ki67) und Amyloid Beta wurden immungefärbt. Die Analyse von Perizytendichte (Perizyten per Volumen Gewebe), linearer Perizytendichte (Perizyten per Kapillarenlänge) und Kapillarendichte (Kapillaren per Volumen Gewebe) wurde mit den stereologischen Methoden Optical Fractionator und Spaceballs durchgeführt. Der Perizytenbesatz (Anteil vom Kapillarenareal das von Perizyten besetzt ist) wurde mit einem Schwellenwertverfahren und Amyloid Beta (Anteil vom Gewebe das von Amyloid Beta besetzt ist) mit dem stereologischen Area Fraction Fractionator Tool gemessen.

Es gab keine signifikanten Unterschiede in der linearen Perizytendichte (Kontrolle vs. AK; Mittelwert ± s; 8,3 ± 0,7 vs. 8,5 ± 1 Zellen / mm Kapillare; $p = 0,4635$) oder dem Perizytenbesatz (Kontrolle vs. AK; Median; 75,6 vs. 75,8 % Areal; $p = 0,7804$) zwischen Kontrollen und AK-Fällen. Verglichen mit Kontrollen waren AK-Fälle charakterisiert durch einen 24%-Anstieg der Kapillarendichte (Kontrolle vs. AK; Mittelwert ± s; 291 ± 39 vs. 361 ± 48 mm / mm^3; $p < 0,0001$), begleitet von einem parallelen 28%-Anstieg der Perizytendichte (Kontrolle vs. AK; Mittelwert ± s; 2412 ± 376 vs. 3081 ± 584 Zellen / mm^3; $p = 0,0006$). Die Erhöhung der Gefäßdichte beschränkte sich auf Kapillaren, andere parenchymale Gefäße waren nicht betroffen. Die Kapillarendichte wies eine starke positive Korrelation mit Gesamt-Amyloid Beta auf (Kontrolle vs. AK; $r_s = 0.6419$, $p < 0.0001$). Proliferierende Perizyten und Endothelzellen waren sowohl bei Kontrollen als auch bei AK-Fällen selten.

Wie unsere Ergebnisse zeigen, ist die AK-Pathologie im mittleren frontalen Kortex durch eine erhöhte Kapillarendichte mit einer morphometrisch normalen Perizytenpopulation charakterisiert. Dies legt nahe, dass die gestörten Blut-Hirn-Schranken und die neurovaskuläre Dysregulation bei der AK-Pathologie nicht durch Perizytenverlust begründet sind.

1. Introduction

1.1. Alzheimer's disease

1.1.1. Epidemiology of Alzheimer's disease

Alzheimer's disease (AD) is considered to be the most frequent type of dementia, accounting for about 50-75% of all dementia cases[1-4].

In 2020, estimates suggested that 1.6 million people with dementia were living in Germany[5-7]. The number of dementia cases is currently rising[5,8]: by the year 2050, the number of people with dementia in Germany is expected to increase to 2.4-2.8 million[5]. The World Alzheimer Report 2019 indicated that worldwide there were approximately 50 million people living with dementia and by 2050 this number is expected to more than triple[6].

The prevalence rate of dementia increases significantly in the older generations, starting with 1.3% in the 65-69 year range and increasing to 40.9% in the >90 year range[5,7].

In the 2020 Alzheimer's Association Report[9], AD was estimated to be a leading cause of disability and poor health. Recent research has ranked AD as the sixth leading cause of death in the United States[1,10,11].

The economic impact of dementia is substantial and growing: in 2019, the global annual cost was estimated at US $1 trillion, which is expected to double by 2030[6].

Altogether, the adverse effect of AD on morbidity and mortality and the growing prevalence rates implicate the major public health impact of AD. These findings highlight the relevance of research to further develop care policies, promote support for affected individuals, and improve prevention and treatment of AD[6].

1.1.2. Alzheimer's pathology

Historically, the term 'Alzheimer's disease' has referred to different aspects of the illness[12]: clinicians, pathologists, and researchers may have referred to clinical dementia presentation, neuropathological findings, or both when they used the term 'Alzheimer's disease'[12]. According to the revised definition of Alzheimer's disease by the International Working Group for New Research Criteria for the Diagnosis of AD, only the neuropathological changes are referred to as 'Alzheimer's pathology'[12]. Analogous to this definition, we use the term 'AD

pathology' to refer to neuropathological changes while 'Alzheimer's disease' or 'AD' encompasses the clinical spectrum of the disorder[12].

Individuals may be diagnosed with AD according to standard diagnostic criteria such as the Diagnostic and Statistical Manual of Mental Disorders (DSM)[13] or the International Statistical Classification of Diseases and Related Health Problems (ICD)[14]. For example, the ICD-10 includes the following main criteria: decline in memory, decline in other cognitive abilities, apathy, and coarsening of social behaviour[14]. These symptoms interfere with everyday activities[14] and typically progress over years with negative impact on psychosocial functioning[1].

AD pathology is characterized by – but not limited to – regional neuropathological findings of increased amyloid beta peptide (Aβ) and neurofibrillary tangles (NFTs)[15]. In 1906, Alois Alzheimer famously first presented his report on plaques in the brain of one of his dementia patients at a lecture in Tübingen, Germany[16]. Almost 80 years later, the peptide Aβ was first described as a crucial component of the plaques[17]. Aβ accumulation is now generally accepted as one of the pathological hallmarks of AD pathology[15]. The deposition of Aβ may be associated with AD pathology, but it also occurs in other disorders such as trisomy 21 and, to a lesser degree, in aging without dementia[18,19].

Aβ is a peptide consisting of 36-43 amino acids and a cleavage product of the transmembrane amyloid precursor protein (APP)[20,21]. APP is assumed to be expressed in most human cell membranes and cleaved enzymatically by α-, β-, and γ-secretases, which produces peptide products of different sizes[20,21,22]. Two of the main Aβ products are the more soluble $A\beta_{40}$ and the less soluble $A\beta_{42}$: the latter, $A\beta_{42}$, is characterized by a higher propensity to fibrilise[22]. These two Aβ products are the result of sequential cleavage of APP by β-secretase and γ-secretase[22].

In the most common variants of AD pathology that are not linked to autosomal-dominant inheritance, it has been hypothesized that a principal pathway for Aβ accumulation is failed clearance[23]. Genome-wide association studies (GWAS) demonstrated that one of the strongest genetic risk factor for AD is the ε4 polymorphism of the APOE gene (APOE4), which may be relevant for clearance of Aβ and lipid metabolism[24]. Potentially dysfunctional Aβ clearance pathways, such as impaired enzymatic degradation, were investigated and several candidate enzymes identified, but the exact mechanism of failed clearance is not fully established[25].

In less common familial variants of AD pathology such as autosomal-dominant genetic mutations of APP, presenilin 1 (PSEN1), and presenilin 2 (PSEN2), an increased production of Aβ may contribute to Aβ accumulation[23].

The role of Aβ in AD pathology has been addressed in the well-known amyloid cascade hypothesis: according to this hypothesis, Aβ accumulation may initiate a cascade of events including (1) microglial and astrocytic activation and increased inflammation, which could lead to (2) oxidative injury, followed by (3) altered kinase/phosphatase activity possibly causing NFTs and eventually resulting in (4) neuronal/synaptic dysfunction, selective neuronal loss, and dementia[23].

The involved pathways and causality of events remain controversial[23], but the accumulation of Aβ and NFTs is considered a hallmark of AD pathology with clinical implications[12]: in addition to clinical dementia assessment, The International Working Group for New Research Criteria for the Diagnosis of AD recommends implementation of diagnostic markers such as $A\beta_{42}$, total tau, and phospho-tau in cerebrospinal fluid; retention of amyloid tracers (positron emission tomography [PET]); medial temporal lobe atrophy (structural magnetic resonance imaging [MRI]); and/or parietal hypometabolism (fluorodeoxyglucose PET)[12].

1.1.3. Microvascular pathology in Alzheimer's pathology

Accumulating evidence suggests that the overlap between AD pathology and vascular pathology is greater than previously thought[26]. The notion that AD pathology is restricted to neuronal pathology is challenged by evidence arising from genetic studies and disease models[26]. Other brain cell types, such as microglia and cells that contribute to the neurovascular unit (e.g. astrocytes and pericytes), appear to be involved in the development of AD pathology as well[26]. A dichotomous division between vascular pathology and AD pathology has been questioned by several authors in recent years[26-29].

Hypotheses such as the 'two-hit hypothesis'[28], 'neurovascular hypothesis'[30], 'critically attained threshold of cerebral hypoperfusion (CATCH)'[31], 'capillary dysfunction hypothesis'[29], and the term 'vasocognopathy'[27] have aimed to capture vascular components in AD pathology into explanatory frameworks. According to these hypotheses, altered perfusion occurs early in the disease progression.

For instance, 'capillary dysfunction' characterized by disturbed blood flow regulation and disruption of the blood-brain barrier (BBB) was hypothesized as an initial event in AD pathology by Ostergaard et al. (2013)[29]. They argue that the cause for capillary compromise

could be related to the risk factors for AD pathology, which have detrimental effects on the microvasculature[29]. Risk factors for AD and other types of dementia include genetic susceptibility genes (e.g. APOE4), aging, positive family history, traumatic brain injury, mid-life obesity, mid-life hypertension, current smoking, and diabetes mellitus[31,32]. It was proposed that these risk factors can cause lesions in microvessels, which may increase the risk of microhemorrhages[33]. Microhemorrhages might not be clinically evident initially, but could accumulate over years and cause hypoxia, disturb Aβ clearance, and thereby drive the development of AD pathology[29,33,34]. Stone (2008) hypothesized that 'the breakdown of large vessels causes stroke, and the breakdown of small vessels is not observed clinically, but leads to dementia and to "pathology of the Alzheimer type" i.e. to the deposition of plaques'[33].

The association between lacunar brain infarction and AD pathology was investigated in another well-known study by Snowdon et al. (1997)[35]. The results of the study indicated that less AD pathology is required for the development of clinical dementia if lacunar infarcts have occurred[35]. Snowdon et al. concluded that vascular pathology has an impact on the occurrence and severity of dementia symptoms in AD[35].

Several structural microvascular alterations have been reported in AD pathology such as increased thickness, inclusions, and vacuolization of the basement membrane[29,36,37], an increase in very thin fibrous processes (termed 'string vessels', typically with a diameter of <1.5µm[36,38]), altered capillary density (discussed in section 4.2.2.)[39-60], and a decrease in capillary diameter[50]. In a post-mortem study, the decrease in capillary diameter explained about half of the cognitive variability in AD subjects[50].

The deposition of Aβ in the vessel walls (cerebral amyloid angiopathy [CAA]) contributes to vascular pathology in AD pathology[61]: post-mortem studies demonstrated that CAA is associated with increased cognitive decline in AD[62]. In AD subjects, the severity of capillary CAA has been positively correlated with the severity of neuropathological measures of AD pathology such as the criteria of the Consortium to Establish a Registry for Alzheimer's Disease (CERAD), Braak and Braak, and The National Institute on Aging and Reagan Institute (NIA-RI)[61,63].

In CAA, Aβ is located in direct vicinity to vascular cellular elements such as pericytes. Since amyloid has been hypothesized to cause degeneration[64] and dysfunction[65] of pericytes, it also raises the question if CAA has a negative impact on pericyte function and survival in AD pathology.

Overall, the literature suggests that microvascular pathology may be an early contributor to the development of AD pathology[26,29].

1.2. Pericytes

1.2.1. Pericyte functions

The pericyte is a microvascular mural cell type with diverse functions: pericytes are considered integral in signalling pathways of angiogenesis and vascular maturation and have been hypothesized to regulate the blood-brain barrier, CBF, stem cell activity, and inflammatory and clearance processes[66,67].

Pericytes were first described in 1871 by Eberth[68]. They became initially known from 1873 as Rouget cells, named after the author of another pioneering publication[69]. Zimmermann eventually coined the name 'pericyte' in 1923[70]. The name 'pericyte' refers to the location of the cell ('-cyte') partially encircling ('peri-') blood vessels[71].

Pericytes are located beneath and in constant contact with the basement membrane (Figure 3)[72]. They are in direct vicinity to endothelial cells and closely connected to astrocytes as the majority of the abluminal pericyte surface is covered with astrocyte endfeet[72]. The pericyte morphology and density depends on the type of microvessel it is located on and the type of organ it is situated in[73]: the retina has one of the highest known pericyte to endothelial cell ratios (1:1) while the skeletal muscle has one of the lowest ratios (1:100)[74].

Capillaries in the central nervous system (CNS) have one of the highest pericyte densities of all capillaries in the human body, perhaps due to their role in maintaining the BBB[73]. The BBB prevents the exchange of ions and small molecules between the CNS parenchyma and blood circulation[75]. Minor alterations in the barrier affect cerebral metabolism and function[75]. Several cell types, such as pericytes and endothelial cells, exert a regulatory role on the BBB in microvessels[67]. For instance, pericytes regulate the expression and alignment of tight junction proteins in the BBB[67]. Pericyte-deficient mouse models have shown disrupted tight junctions, which may cause increased vascular permeability to potentially toxic molecules[76]. Altogether, pericytes are considered important in keeping the BBB intact[67].

Morphologically, pericytes exhibit primary axillar processes and shorter secondary perpendicular processes on their main location on capillaries[66]. The short perpendicular processes typically do not encircle the complete circumference of the capillary[71]. This incomplete encirclement is considered by some authors to be a specific characteristic of pericytes[66]. However, a morphological continuum appears to exist between pericytes on

capillaries, ‘spindle-shaped’ smooth muscle cells on arterioles, and ‘stellate-shaped’ smooth muscle cells on venules[66]. The so-called ‘cyto-architectural continuum’[66] seems particularly apparent on vessels closest to capillaries such as precapillary arterioles and postcapillary venules invested with phenotypically ‘transitional’ mural cells[77]: these ‘transitional’ mural cells share phenotypical features with both pericytes and smooth muscle cells[77].

In fact, pericytes and vascular smooth muscle cells are related functionally and developmentally[66]. The existence of contractile proteins such as vimentin and myosin were detected in both pericytes and smooth muscle cells, which may indicate abilities to contract and regulate blood flow[78]. In the forebrain, pericytes and vascular smooth muscle cells both originate embryologically from the ectoderm-derived neural crest[66].

Pericytes appear to have multipotent progenitor potential as they share multipotent features at the clonal level and expression of common markers with mesenchymal stem cells[79]. Cultured primary pericytes from ischemic regions in the mouse brain differentiated into both vascular and neural cells and showed a complex phenotype of angioblasts[79]. A recent study, however, has challenged the role of pericytes as multipotent progenitors because endogenous pericytes did not behave as mesenchymal stem cells in vivo[80]. The authors of the recent study argue that the plasticity of pericytes observed in previous studies may have been caused by manipulations during ex vivo treatment of the cells[80].

Pericytes are involved in inflammatory processes as primary human pericyte cultures respond to cytokine challenge with immune activation[81]. For example, pericytes regulated leukocyte adhesion and migration across the BBB in a transgenic mouse model[82]. Pericytes also contribute to clearance processes as they exhibit ‘macrophage-like’ properties, can induce phagocytosis, present antigen, and have larger amounts of lysosomes to clear tissue debris and proteins[83].

Results from murine studies indicate that pericytes influence angiogenesis and endothelial cell survival: depending on the degree of pericyte deficiency in these mouse models, hyperproliferation or regression of vessels occurred, which suggests a regulatory effect of pericytes on angiogenesis and maintenance of the vasculature[84,85].

CBF can be altered according to regional demand in the brain[86]: an increased blood flow as a response to neuronal activation is referred to as ‘functional hyperemia’[86]. Pericytes on vessels smaller than penetrating arterioles were regarded as regulators of blood flow during ‘functional hyperemia’ in mouse models[87]. Pericyte contraction may be modulated by mediators from astrocytes (e.g. arachidonic acid and prostaglandin E_2) and neurons (e.g. nitric oxide, glutamate, adenosine, and norepinephrine)[67]. The role of pericytes for the regulation of CBF is possibly

not the same in all vascular segments since the expression of certain contractile proteins (e.g. α–smooth muscle actin) in mural cells changes according to the type of vessel[71].

Pericytes also appear to contribute to CBF disturbances under pathological circumstances: in ischemia, even after reperfusion of proximal arteries, rigorous constriction of pericytes was detected, which may impair capillary reflow[88].

Conversely, a significant involvement of pericytes in functional hyperemia and stroke is questioned by results of another study that did not show pericyte but only smooth muscle cell contractility in normal and ischemic mice brains[89]. These findings suggest that the exact role of pericytes for CBF regulation under physiological and pathological circumstances is not fully elucidated.

The pericyte functions presented in this section open up the prospect to question the role of pericytes in AD pathology because disturbed CBF, BBB impairment, and neurovascular dysfunction have been reported to occur in AD pathology[28,65,75,85].

1.2.2. Pericyte deficiency as a potential contributor to AD pathology

Pericytes are considered to be integral in maintaining the BBB[90]. This was demonstrated in a mouse model of pericyte deficiency, causing increased permeability to high- and low-molecular mass tracers by endothelial transcytosis[90]. Pericyte deficiency caused a defect in the polarization of astrocyte end-feet surrounding microvessels and a downregulation of BBB-specific gene expression in endothelial cells[90]. This process was also suspected as a potential cause for increased BBB permeability in human AD pathology[26]. Furthermore, pericyte loss in a murine model of AD pathology was followed by diminished Aβ clearance via interstitial fluid, an increase in amyloid angiopathy and NFTs, and early neuronal loss with cognitive decline[91].

A disrupted coupling between neuronal stimuli and capillary blood flow responses, so-called ‘neurovascular uncoupling’, resulting in reduced cerebral oxygen supply has been detected in a recent ‘loss-of-function’ pericyte-deficient mouse model[92]. ‘Neurovascular uncoupling’ has also been hypothesized in AD pathology[26]. This raises the question of a role of pericytes in the development of AD pathology[26].

However, the relevance of pericyte deficiency for cognitive function remains uncertain as other studies have failed to show a significant correlation between pericyte degeneration and cognitive decline[93]. In one study, hypoxia-induced pericyte degeneration did not significantly correlate with cognitive impairment in rats and the authors concluded that ‘pericytic pathology

does not directly interfere with memory formation'[93]. In another study, reduced pericyte coverage in aged mice was not related to neurovascular function[94].

Further research is needed to determine if pericyte deficiency plays a crucial role in the development of cognitive decline in AD.

1.2.3. Pericyte population in AD pathology

Variants of Aβ have toxic effects on cultured pericytes[64]. In a study with cultured cells, pericytes showed morphological signs of degeneration after exposure to Aβ medium[64]. Notably, pericytes degenerated twice as rapidly as leptomeningeal smooth muscle cells, suggesting a vulnerability of pericytes to toxic effects of Aβ[64].

In human AD samples, electron microscopy studies showed morphological signs of degeneration in pericytes such as increased intracellular lipofuscin-like material and damaged mitochondria[37,95,96]. These findings indicate an association between amyloid deposition and pericyte degeneration in human AD pathology.

In contrast, Farkas et al. (2000) did not detect evidence of pericyte degeneration in human AD pathology[97]. They found no change in number of degenerating pericytes in AD subjects compared to age-matched controls[97]. They concluded that pericyte degeneration does not play a causal role in AD pathology and vascular lesion is restricted to the basement membrane[97].

It has even been hypothesized that pericytes could proliferate or increase in coverage to compensate for the dysfunctioning BBB in AD pathology[36,99,100] since an increase in pericyte coverage is generally considered an 'indicator of vascular dysfunctioning' in other illnesses such as pulmonary hypertension or acoustic trauma to the cochlea[101,102].

In conclusion, whether pericyte loss or proliferation is a feature of AD pathology is not clear[75]. A systematic analysis of the pericyte population could promote our understanding of the microvascular contribution to AD pathology.

1.3. Study objectives

As described in the sections above, several studies and reviews[28,37,95,96], albeit not all[97,100], have suggested pericyte degeneration and loss in AD pathology. However, quantitative studies on pericyte density and coverage have been few and have shown heterogenous results ranging from pericyte loss to increase in pericyte coverage (discussed in sections 1.2.3. and 4.2.1.)[51,52,59,97,100,103].

To our knowledge, no previous studies on pericytes implemented stereological methods of quantification. Stereological methods are proposed as a 'gold standard' of quantitative microscopy and intended to reduce methodological bias[104].

1.3.1. Primary objective, hypothesis, and outcome measure

Objective 1

The primary objective of our study was to determine if pericyte loss occurs in AD pathology.

- Hypothesis 1: pericyte loss occurs in AD pathology.

We aimed to assess the hypothesis by stereological analysis of pericyte linear density in middle frontal gyrus sections from human AD cases compared with control cases. Pericyte linear density (number of pericytes per capillary length) was our primary outcome measure and it was calculated from pericyte density (number of pericytes per tissue volume) and capillary density (capillary length per tissue volume).

In an exploratory analysis, we compared the primary outcome measure pericyte linear density between AD subjects that were stratified by neuropathological and genetical characteristics: we anticipated decreased pericyte linear density in subjects with the APOE4 allele compared with subjects with the APOE2-3 allele. We also expected decreased pericyte linear density in subjects with higher scores (i.e. higher severity) of neuropathological measures (CERAD, NFTs, atrophy, and capillary CAA) compared with subjects with lower scores of neuropathological measures.

In another exploratory analysis, we correlated pericyte linear density with total Aβ (% area) and anticipated a negative correlation.

1.3.2. Secondary objectives, hypotheses, and outcome measures

Objective 2

It was our objective to identify if pericyte coverage on capillaries is decreased in AD pathology.

- Hypothesis 2: pericyte coverage is decreased in AD pathology.

Decreased pericyte coverage may potentially indicate pericyte degeneration in AD pathology. Accordingly, we examined the outcome measure pericyte coverage on capillaries (percentage of capillary area covered by pericytes).

Objective 3

It was our objective to detect if pericyte proliferation is decreased in AD pathology.

- Hypothesis 3: pericyte proliferation is decreased in AD pathology.

Decreased pericyte proliferation may possibly be associated with pericyte degeneration in AD pathology. We examined the outcome measure pericyte proliferation (proliferating pericytes per capillary length).

Objective 4

We aimed to investigate whether microvascular lesions in AD pathology are limited to pericytes or if they affect the density of the microvascular network as well. It was our objective to determine if the capillary density is decreased in AD pathology.

- Hypothesis 4: capillary density is decreased in AD pathology.

The outcome measure was capillary density (capillary length per tissue volume). The capillary diameter was defined as ≤9µm.

In an exploratory analysis, we determined the density of vessels larger than capillaries including 'intermediate vessels' with a diameter >9 & ≤50µm (e.g. precapillary and small arterioles and postcapillary and small venules) and 'large vessels' with a diameter >50µm (e.g. arterioles and venules)[105]. We expected the largest decrease in vessel density in the capillary segment of the microvascular network in AD pathology.

Objective 5

It was our objective to investigate if endothelial cell proliferation is decreased in AD pathology.

- Hypothesis 5: endothelial cell proliferation is decreased in AD pathology.

Decreased endothelial cell proliferation may possibly be associated with endothelial cell degeneration in AD pathology. The outcome measure was endothelial cell proliferation (proliferating endothelial cells per capillary length).

2. Methods

2.1. Subjects

The study included specimens from 16 control and 16 AD subjects. Samples were provided by the New Zealand Neurological Foundation Human Brain Bank, Centre for Brain Research, University of Auckland in Auckland, New Zealand. Specimens were obtained from the Auckland City Hospital after informed consent of the subject in compliance with ethical and legal guidelines and approval by the institutional review board. Records of the clinical history and autopsy are summarized in Table 1.

All AD subjects had a diagnosis of AD that was neuropathologically confirmed. Control subjects showed no clinical signs of dementia (confirmation by the general practitioner).

The brain bank provided us with sex, age, post-mortem time, and cause of death for all subjects. Groups were matched for sex and age (results of matching are reported in section 3.1.).

The brain bank also provided us with estimates of dementia duration and neuropathological measures such as the CERAD score (neuritic plaque score: absent, sparse, moderate, or frequent), four-tier NFT score (absent, mild, moderate, or severe), and four-tier atrophy score (absent, mild, moderate, or severe) for AD subjects[106].

APOE genotyping was done by our collaboration partner at the Department of Translational Neuroscience, University Medical Center (UMC) Utrecht Brain Center, Utrecht University in Utrecht, The Netherlands (genotyping methods are reported in our publication[107]).

Other neuropathological measures such as total Aβ (% area), vascular Aβ (% area), and capillary cerebral amyloid angiopathy (positive or negative) were established in our laboratory (methods are described in sections 2.2.2. and 2.3.7.).

Table 1. Neuropathological and clinical characteristics of subjects.

Case	Brain bank ID	Group	Age (y)	Sex	PMT (h)	APOE genotype	Atrophy	Dementia duration (y)	NFT score	Neuritic plaque score (CERAD)[106]	Capillary CAA[62]	Cause of death
1	H122	CTRL	72	F	9	E3/E3	n.d.	0	n.d.	n.d.	Neg.	Emphysema
2	H109	CTRL	81	M	7	E3/E3	n.d.	0	n.d.	n.d.	Neg.	Coronary atherosclerosis
3	H110	CTRL	83	F	14	E2/E2	n.d.	0	n.d.	n.d.	Neg.	Ruptured aortic aneurysm
4	H137	CTRL	77	F	12	E3/E4	n.d.	0	n.d.	n.d.	Neg.	Coronary atherosclerosis
5	H131	CTRL	73	F	13	E3/E3	n.d.	0	n.d.	n.d.	Neg.	Ischemic heart disease
6	H150	CTRL	78	M	12	E3/E3	n.d.	0	n.d.	n.d.	Neg.	Ruptured myocardial infarct
7	H123	CTRL	78	M	7.5	E2/E3	n.d.	0	n.d.	n.d.	Neg.	Ruptured aortic aneurysm
8	H103	CTRL	70	M	5	E3/E3	n.d.	0	n.d.	n.d.	Neg.	Myocardial infarct
9	H79	CTRL	75	M	11	E3/E3	n.d.	0	n.d.	n.d.	Neg.	Myocardial infarct
10	H77	CTRL	75	M	3.4	E3/E4	n.d.	0	n.d.	n.d.	Neg.	Aortic aneurysm
11	H241	CTRL	76	F	12	E3/E4	n.d.	0	n.d.	n.d.	Neg.	Metastatic bowel cancer
12	H190	CTRL	72	F	19	E3/E3	n.d.	0	n.d.	n.d.	Neg.	Ruptured myocardial infarct
13	H181	CTRL	78	F	20	E3/E3	n.d.	0	n.d.	n.d.	Neg.	Aortic aneurysm
14	H238	CTRL	63	F	16	E3/E3	n.d.	0	n.d.	n.d.	Neg.	Dissecting aortic aneurysm
15	H164	CTRL	73	M	13	E3/E3	n.d.	0	n.d.	n.d.	Neg.	Ischaemic heart disease
16	H152	CTRL	79	M	18	E3/E3	n.d.	0	n.d.	n.d.	Neg.	Congestive heart failure
17	AZ46	AD	82	F	22	E4/E4	1	n.d.	2	2	Neg.	Coronary artery disease
18	AZ37	AD	83	M	4	E3/E4	3	n.d.	1	2	Pos.	Bronchopneumonia
19	AZ33	AD	65	M	20	E3/E3	1	7	1	2	Neg.	Hypostatic pneumonia
20	AZ22	AD	81	F	2	E2/E3	1	10	2	2	Pos.	Bronchopneumonia
21	AZ20	AD	72	F	3	n.d.	3	7	2	3	Neg.	Cachexia
22	AZ34	AD	74	F	18	n.d.	2	5	2	2	Neg.	Bronchopneumonia, breast carcinoma
23	AZ29	AD	76	F	20	n.d.	2	n.d.	2	2	Pos.	Pneumonia
24	AZ32	AD	75	F	3	n.d.	2	n.d.	1	2	Neg.	Bronchostatic pneumonia
25	AZ28	AD	75	F	8	n.d.	1	4	2	2	Neg.	Pneumonia
26	AZ23	AD	71	F	10	E3/E4	1	2	2	2	Neg.	Bronchopneumonia
27	AZ38	AD	80	M	5.5	E3/E3	2	17.5	2	3	Neg.	Respiratory arrest / pulmonary edema
28	AZ39	AD	74	M	12	E3/E3	1	20	2	2	Neg.	Sepsis
29	AZ80	AD	77	M	4.5	E3/E4	3	13	3	3	Neg.	Myocardial infarct
30	AZ90	AD	73	M	4	E3/E3	3	n.d.	3	3	Neg.	Gastrointestinal hemorrhage
31	AZ43	AD	80	M	21	n.d.	1	n.d.	2	2	Neg.	Bronchopneumonia
32	AZ88	AD	83	M	21	E3/E3	2	n.d.	3	3	Neg.	Pneumonia

Abbreviations: y, years; h, hours; CTRL, control subject; AD, subject with Alzheimer's disease; PMT, post-mortem time; APOE, apolipoprotein E; NFT, neurofibrillary tangles; CERAD, Consortium to Establish a Registry for Alzheimer's Disease[106]; CAA, cerebral amyloid angiopathy[62]; atrophy and NFT score 1, mild; 2, moderate; 3, severe; neuritic plaque score (CERAD[106]) 0, absent; 1, sparse; 2, moderate; 3, frequent; capillary CAA[62] pos., positive; neg. negative; n.d., not determined due to insufficient material quantity[107].
Table 1 is adapted from our publication[107].

2.2. Stainings

Fresh frozen (-80°C) specimen blocks were cut orthogonal to the middle frontal gyrus with a cryostat (Leica CM3050 S, Leica Biosystems, Nussloch, DE). The thickness of all sections was 60µm.

2.2.1. Immunofluorescence stainings

If not mentioned otherwise, the staining procedures were performed at room temperature and a washing step with three changes of tris-buffered saline (TBS) was included between each step. TBS was made from 50mM TrisHCl and 150mM NaCl and adjusted to pH 7.4 with HCl (if not otherwise specified, all chemicals by Roth, Karlsruhe, DE). The liquid blocker PAP-pen (Science Services, München, DE) was used in all stainings to prevent any spillover of the applied solutions. The fresh frozen mounted slices were fixed for 10 minutes in 100% methanol at -20°C. Only slices stained for the proliferation marker Ki67 were fixed for 10 minutes in ice-cold 4% paraformaldehyde (PFA) instead of methanol.

Blocking of the unspecific binding sites was done for one hour in the host species serum of the second antibody: 10% normal donkey serum (NDS; Vector Laboratories, Burlingame, USA), 0.3% Triton X-100 (Sigma Aldrich, Steinheim, DE) for membrane permeabilization, and TBS. The first antibodies were incubated overnight at 4°C in 1% NDS, 0.3% Triton X-100, and TBS.

Vasculature was identified by laminin immunoreactivity (1:800, mouse anti-human, γ1, clone 2E8; Millipore, Schwalbach, DE). Pericytes were characterized by PDGFRβ immunoreactivity (1:100, rabbit anti-human, Y92, C-term; Genetex, Irvine, USA).

The Ki67 (marker for proliferation) staining was performed analogous to the above-mentioned staining steps except that the rabbit anti-Ki67 antibody (1:1000; Abcam, Cambridge, UK) was used instead of the PDGFRβ antibody.

In all immunofluorescence stainings, the secondary antibodies Alexa 488-conjugated donkey anti-mouse (1:1000; Invitrogen, Karlsruhe, DE) and Alexa 568-conjugated donkey anti-rabbit (1:1000; Invitrogen, Karlsruhe, DE) were incubated in 5% NDS, 0.3% Triton X-100, and TBS for 4 hours. All slices were washed in three changes of TBS for 10 minutes each and 4',6-diamidino-2-phenylindole (DAPI, 1:60.000; Sigma Aldrich, Steinheim, DE) was added to the

second wash for nuclear labelling. Fluorsave was used as the embedding medium (Vector Laboratories, Burlingame, USA).

2.2.2. Immunoperoxidase staining

This staining was used for stereological quantification of Aβ. The fresh frozen mounted slices were fixed for 15 minutes in 100% methanol at -20°C. Endogenous peroxidase was inactivated for 15 minutes in 0.3% H_2O_2 and TBS. Unspecific binding sites were blocked for two hours with 10% normal horse serum (NHS; Vector Laboratories, Burlingame, USA), 0.3% Triton X-100, and TBS. Aβ was stained with amyloid beta antibody (1:500, mouse anti-human, clone DE2B4; Santa Cruz, Heidelberg, DE) that was incubated overnight at 4°C in 1% NHS, 0.3% Triton X-100, and TBS. The secondary biotinylated horse anti-mouse antibody (1:200) in 1% NHS, 0.3% Triton X-100, and TBS was incubated for 4 hours at room temperature. The avidin-biotin complex (ABC) kit (Vector Laboratories, Eching, DE) was used according to the manufacturer's instructions. Slices were washed in three changes of tris-buffer (TB) for 10 minutes. The 3,3'-diaminobenzidine (DAB) kit (Sigma Aldrich, Steinheim, DE) was also used according to the manufacturer's instructions and incubated for three minutes. Slices were washed in three changes of TB for 10 minutes each and air-dried.

Nuclei were stained with Harris' haematoxylin (Morphisto, Frankfurt am Main, DE) after Aβ staining: slices were immersed in 100% ethanol for 10 minutes and rehydrated by a graded alcohol series. Bidistilled water was used for washing. Slices were immersed in Harris' haematoxylin for five minutes and differentiated in 1% HCl-ethanol for one second. Lukewarm ammonia water (1% $NaHCO_3$) was used for bluing (3 minutes).

As a final step, slices were dehydrated in a graded alcohol series and kept in Rotihistol (Roth, Karlsruhe, DE) until they were embedded in Rotihistokit (Roth, Karlsruhe, DE) and coverslipped.

For illustration purposes, we performed another immunoperoxidase staining of the vasculature. This staining of the vasculature was performed analogous to the Aβ staining except that a laminin antibody (1:800, mouse anti-human, γ1, clone 2E8; Millipore, Schwalbach, DE) was used instead of the amyloid beta antibody and nuclei were not stained.

2.3. Morphometric analyses

2.3.1. Stereology

Stereology can be defined as a method that provides 'meaningful quantitative descriptions of the geometry of 3D structures from measurements that are made on 2D images'[108].

The stereological analyses included samples from 32 subjects (AD n = 16 vs. control n = 16) and were performed with the Stereoinvestigator 10 software (MBF Bioscience, Magdeburg, DE). If not mentioned otherwise, we included three slices per subject. For multiple slices, we analysed every second consecutive slice of the tissue block. The slices were alternating and not neighbouring to avoid multiple counting of structures located on the edge. The investigator was blinded to the ID of the sample under scrutiny.

First, the grey matter of the middle frontal gyrus was chosen as the single region of interest (ROI) and delineated by the white matter. The grey matter could be differentiated in the DAPI or haematoxylin stainings with a low-resolution 10× / numerical aperture (NA) 0.30 dry objective lens (microscope Leica DMIL, fluorescence filters F41-025, F41-027, and F41-041; all lenses by Leica Camera AG, Wetzlar, DE). The height of each fluorescence-stained slice was determined individually with the same setup and high-resolution 40× / NA 1.25-0.75 oil immersion objective used for stereological analysis. The first nucleus in focus at the top and the last nucleus in focus at the bottom defined the height of the slice. The average post-processing mounted thickness (t) of the tissue was sampled at 6-7 different points within the ROI and averaged[41].

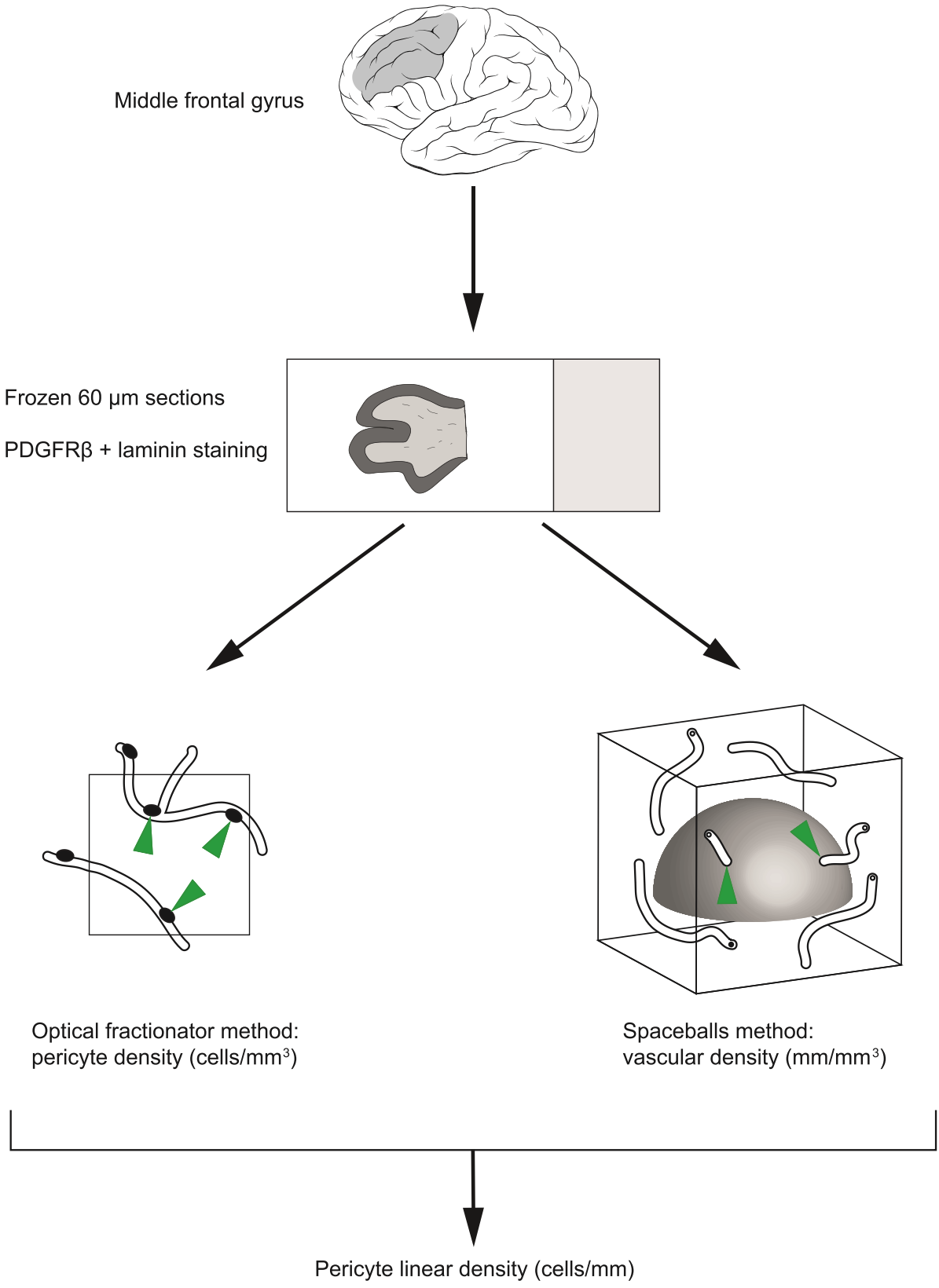

Figure 1. *Stereological method of pericyte quantification*. Frozen 60 µm sections from the middle frontal gyrus were mounted onto slides and stained. PDGFRβ immunoreactivity indicated pericytes. Laminin immunoreactivity indicated the basement membrane of the vasculature. The stereological method optical fractionator[109] was used to measure pericyte

density (number of pericytes per tissue volume; cells/mm^3). The stereological spaceballs method[110] was used to measure the density of the vasculature (vascular length per volume; mm/mm^3). Pericyte linear density was calculated from the above measurements (number of pericytes per capillary length; cells/mm). Green arrowheads indicate counted pericytes (optical fractionator method) and counted vascular intersections (spaceballs method). Figure 1 is adapted from our publication[107].

2.3.2. Pericyte density and linear density

Pericytes were defined as PDGFRβ$^+$ cells with round or oval nuclei embedded in the laminin$^+$ basement membrane that cause an exterior convex protrusion in the vessel wall[66]. The marker PDGFRβ is characteristic of but not exclusive to pericytes[132]. A high-resolution 40× / NA 1.25-0.75 oil immersion objective was used for stereological analysis. Confocal images (Leica SP5 confocal microscope, Wetzlar, DE) were acquired for illustration purposes.

Pericyte density and linear density were measured on three slices per subject (Figure 1). The three-dimensional counting space was projected into the slices and all counting was restricted to its boundaries. In the x-y plane, the counting space consisted of two inclusion and two exclusion lines creating a 120×120µm square (i.e. counting frame). The area of the counting frame (14400µm^2) was chosen to fit ~2 pericytes per counting frame[111]. Every pericyte within the counting frame or touching the inclusion line was included; likewise, every pericyte outside the counting frame or touching the exclusion line was excluded. We counted ~450 pericytes per subject (>200 sampling sites per subject)[112]. The height of the counting space did not include the entire thickness of the slices. The z-plane 3µm guard zones were placed at the upper edge of the counting frame resulting in ~3µm guard zones at the bottom edge, depending on the height of the counting space. Guard zones accounted for possible cutting artefacts and lost nucleoli at tissue borders due to processing[113]. Tissue section fraction (tsf) was defined as the counting space height fraction of the mounted thickness[111].

A lattice, the so-called sampling grid, was superimposed randomly onto the slices by the stereoinvestigator software. A counting space was placed at each intersection of the sampling grid. A total of ~100 counting spaces was projected onto each slice: the x- and y-distances between each counting space in the sampling grid were fitted automatically with respect to the size and shape of the ROI. The sampled fraction of the ROI was defined as the area sampling fraction (asf)[111]. The asf varied between subjects, depending on the size of the ROI. Guard zone and counting frame measures were identical within and between subjects. The height of the counting space and x- and y-distances were identical within subjects and fitted according to

changing ROI measures between subjects. Pericyte counts from all counting spaces on one slice ($\sum Q^-$) were used to estimate the total number of pericytes in the ROI on the same slice (N)[111]:

$$N = \sum Q^- \times \frac{1}{\text{tsf}} \times \frac{1}{\text{asf}} \times \frac{1}{\text{ssf}}$$

The interval of sections sampled, section sampling fraction (ssf), was 1 as the pericyte population was calculated individually for all three slices. Pericyte density was calculated as number of pericytes per tissue volume (cells/mm^3).

Pericytes are located on capillaries and a change in capillary density would likely cause a change in pericyte density. To account for this association, the total number of pericytes was divided by the total capillary length resulting in the pericyte linear density (pericyte cells/mm capillary). Mean pericyte linear density of all three slices was used to calculate pericyte linear density for one subject.

2.3.3. Capillary density

Capillaries were defined as every laminin$^+$ tubular structure with a diameter ≤9µm[114]. A high-resolution 40× / NA 1.25-0.75 oil immersion objective was used for stereological analysis. Capillary diameter (∅) was measured with the 'fast measure tool' provided by the stereoinvestigator software[114].

We determined capillary density with the spaceballs method[110] (Figure 1). Capillary density was determined on the same slices, in the same ROI, and at the same x- and y-distances as pericyte density to provide comparable sampling. Guard zone size was set at 3µm and chosen to account for variability of mounted thickness of the slice and size of the capillary (≤9µm)[110]. A hemisphere, instead of a sphere, was chosen to maximize the number of counts while still maintaining isotropy[110]. The hemispheres were projected into the slices according to the predetermined x- and y-distances. Every intersection between a hemisphere and a capillary was counted. Capillaries were only counted if the hemisphere intersected the central axis of the capillary[114]. We estimated the capillary density according to the following formula[114] (∑is = capillary intersections with the edge of the hemisphere; D_x = sampling grid distance in x; D_y = sampling grid distance in y; t = mounted thickness of the slice; r = radius of the hemisphere; and V = volume of the ROI after cutting):

$$\text{Capillary density} = \frac{2 \times \sum is \times \left(D_x \times D_y \times t\right)}{2 \times \pi \times r^2} \times \frac{1}{V}$$

2.3.4. Intermediate and large vessel density

Intermediate and large vessel densities were estimated on the first of the three slices used for estimation of capillary density. We divided the microvascular network into a group of laminin$^+$ 'intermediate' vessels with a diameter >9 & ≤50µm (e.g. precapillary and small arterioles and postcapillary and small venules) and 'large' vessels with a diameter >50µm (e.g. arterioles and venules)[105].

The lenses, guard zones, grey-matter-ROI, and spaceballs formula were the same as in the capillary density estimation. Vessels with a diameter >9 & ≤20µm were counted as described for the capillaries.

For this study, we established a novel protocol for counting vessels with a diameter >20µm because the regular spaceballs protocol is less efficient for these infrequent events. Vessels within the grey-matter-ROI with a larger diameter than that of capillaries were preselected with additional ROIs. For this purpose, we used a low-resolution 10× / NA 0.30 dry objective lens. These additional ROIs encircled each vessel with a larger diameter than that of capillaries and excluded most of the parenchyma. To increase counting efficiency, we only projected the hemispheres into the additional ROIs. Intersections between a vessel with a diameter >20µm and a hemisphere were counted[114]. Vessel diameter was determined with the 'fast measure tool' provided by the stereoinvestigator software. We chose small x- and y-distances (100µm) to achieve a large number of intersections between the included vessels and hemispheres within the additional ROIs; x- and y-distances were adjusted in two subjects due to ROI size differences (AD case number 21: 50µm. Control case number 6: 150µm). A vessel was only counted if the central axis of the vessel intersected with the hemisphere.

2.3.5. Pericyte and endothelial cell proliferation

Ki67 analysis was performed on a single slice per subject with a high-resolution 40× / NA 1.25-0.75 oil immersion objective. Confocal images (Leica SP5 confocal microscope) were acquired for illustration purposes. To avoid missing any rare proliferating cells, we performed a meander scan and analysed the entire ROI (grey matter) meandering from side to side and top to bottom

(asf = 1). We counted the proliferating cells and determined two subgroups for analysis: endothelial cells and pericytes. Endothelial cells and pericytes were distinguished based on their morphology and location: pericyte nuclei were identified as round or oval causing an exterior convex protrusion in the vessel wall[66] and differentiated from endothelial cell nuclei, which were plane and longitudinal (width and height <6µm, length 10-15µm)[115]. Ki67$^+$ vascular nuclei below the basement membrane and near the central axis of the vessel were regarded as proliferating intraluminal cells and excluded from the analysis. Proliferating pericytes were divided by capillary length (measured on the same section), which resulted in proliferating pericytes per capillary length; likewise, we divided proliferating endothelial cells by capillary length, which resulted in proliferating endothelial cells per capillary length.

2.3.6. Pericyte coverage

Pericyte coverage was estimated on a single section per subject. The analysis was performed on the first of the three sections per subject included in the pericyte density, pericyte linear density, and capillary density estimation to establish comparable sampling. As reported earlier in the optical fractionator step, a sampling grid was superimposed on the grey matter, thereby creating uniform distances between each sampling site. Two images were captured at each intersection of the sampling grid with a high-resolution 100× / NA 1.4 oil-immersion objective lens. A total of ~10 intersections was sampled per subject.

The first image was collected with a detector channel that filtered the emission spectra of the green fluorescent laminin$^+$ vessels (Alexa Fluor 488). Images with vessels larger than capillaries were excluded. The offset, gain, and exposure time were equal for all Alexa Fluor 488 images.

The second image was collected with a detector channel that filtered the emission spectra of the red fluorescent PDGFRβ$^+$ pericytes (Alexa Fluor 568). The offset, gain, and exposure time were equal for all Alexa Fluor 568 images.

The captured images (fluorescence Red-Green-Blue [RGB] colour) were imported to the image processing software ImageJ (v1.51s). Images were converted to 8-bit greyscale. Manual thresholds were used to create binary black and white images to differentiate between capillary and pericyte signals versus background. First, we determined the area covered by capillary signal (regardless of pixel size or circularity) on all images per subject. Then we determined the area covered by pericyte signal (regardless of pixel size or circularity) on all images per subject. We only included pericyte signals that colocalized with the capillary signal to minimize

background signal interference. We calculated the pericyte coverage as percentage of capillary area covered by pericyte area.

2.3.7. Aβ

Aβ immunohistochemistry was performed on a single section per subject. A 20× / NA 0.5 dry objective lens was used for stereological analysis. We employed the stereological area fraction fractionator tool[116]. As described in the spaceballs and optical fractionator method, a lattice, the so-called sampling grid, was superimposed randomly onto the slice by the stereoinvestigator software. A total of ~200 counting grids per subject was projected into the counting space at each crossing of the lattice. The counting grid divided the image into small squares. The area of each square in the counting grid was always identical: a(p) = 20 × 20µm. $A\beta^+$ squares from all sites collectively (vascular and parenchymal) were used to calculate 'total Aβ'. $A\beta^+$ squares from vascular sites were used to calculate 'vascular Aβ'. The result of the analysis was the $A\beta^+$ area fraction in percent ($A_{\%}$) of the total grey matter area (ROI_A)[116]:

$$A_{\%} = \frac{1}{asf \times a(p) \times P(Y_i)} \times \frac{100}{ROI_A}$$

In each subject, we determined whether the Aβ signal was present in any capillary (i.e. capillary CAA positive/negative)[62]: we performed a meander scan and analysed the entire ROI (grey matter) and a subject was categorized as capillary CAA positive if at least one capillary was CAA positive.

2.4. Statistics

We carried out a sample size estimate for a one-way multivariate analysis of variance (MANOVA), which was based on the following parameters: number of groups = 2 (AD and control); number of response variables = 5 (pericyte density, pericyte linear density, capillary density, intermediate vessel density, and large vessel density); alpha = 0.05; power = 0.9; Pillai's V = 0.45; and effect size $f^2 = 0.82$[41,43,44,100] (G*Power 3.1; Faul, Erdfelder, Buchner, and Lang, DE). The sample size estimate yielded an estimated sample size of N = 28 subjects. The total sample size included in this study (N = 32) exceeded the estimated sample size (N = 28).

Prior to statistical analysis, we assessed the general assumptions[117-119] of the statistical tests. For instance, we used the Shapiro-Wilk test to assess normal distribution and the Levene's test to assess equality of variances[117-119].

One-way MANOVA was used to investigate the effect of diagnosis (control vs. AD) on the following combined microvascular variables: pericyte density, pericyte linear density, capillary density, intermediate vessel density, and large vessel density. Only a significant result in the multivariate analysis was followed by univariate analyses (one-way ANOVAs) for each microvascular variable.

The non-parametric Mann-Whitney U test was used to investigate the effect of variables with two groups on the non-normally distributed variables[118].

The non-parametric Kruskal-Wallis H test was performed to determine the effect of variables with more than two groups on the non-normally distributed variables. Only a significant Kruskal-Wallis H test was followed by post hoc tests for pairwise comparisons of the groups.

Spearman's rank-order correlation was used to investigate the correlations between variables if at least one of the variables was non-normally distributed.

Mean and standard deviation of the mean is expressed as mean ± standard deviation for normally distributed variables. The median and the interquartile range (IQR) is reported for non-normally distributed variables.

For box plots, median is indicated by a horizontal red line, 25th and 75th percentiles are displayed as a box, 5th and 95th percentiles are displayed as whiskers, and individual subjects are indicated by circles.

A p value below 0.05 was considered significant in this exploratory study[119]. According to the recommendations by Althouse (2016)[149] for exploratory studies, the alpha level was not adjusted for multiple comparisons. Based on the recommendations by the American Psychological Association (APA), p values below 0.0001 are reported as < 0.0001, while all other p values are reported exactly with four decimals[120].

Statistical tests were performed with SPSS (version 23, IBM, Ehningen, DE), Matlab (version R2012, Mathworks, Natick, USA), and Microsoft Excel (version 16, Microsoft, Redmond, USA). The Adobe Illustrator CS6 (Adobe Systems GmbH, München, DE) and ImageJ version 1.51s (ImageJ Developers, Bethesda, USA) were used for graphics and illustrations.

3. Results

3.1. Neuropathological and clinical characteristics of subjects

The study included specimens from a sample of 16 control and 16 AD subjects. Sex distribution was equal within and between groups (control: 8 females and 8 males; AD: 8 females and 8 males; Table 1).

The median age was 75.5 years (IQR 5.3) in the control group and 75.5 years (IQR 6.5) in the AD group ($U = 112.5$, $z = -0.586$, $p = 0.5641$; Mann-Whitney U test).

The median post-mortem time was 12 hours (IQR 5.9) in control and 9 hours (IQR 16) in AD cases ($U = 114$, $z = -0.529$, $p = 0.6156$; Mann-Whitney U test).

Compared to control subjects, total Aβ was increased in AD subjects: total Aβ varied from 0 to 1.02% (median 0.18%, IQR 0.39) in the control group and from 0.54 to 2.19% (median 0.91%, IQR 0.60) in the AD group ($U = 27$, $z = -3.810$, $p = 0.0001$; Mann-Whitney U test; Figure 2).

Compared to control subjects, vascular Aβ was increased in AD subjects: there were no signs of vascular Aβ in control cases (median 0%, IQR 0) and vascular Aβ varied from 0 to 0.86% (median 0.07%, IQR 0.18) in AD cases ($U = 24$, $z = -4.407$, $p < 0.0001$; Mann-Whitney U test; Figure 2).

Capillary CAA was negative in all 16 control subjects and positive in 3/16 AD subjects (Table 1).

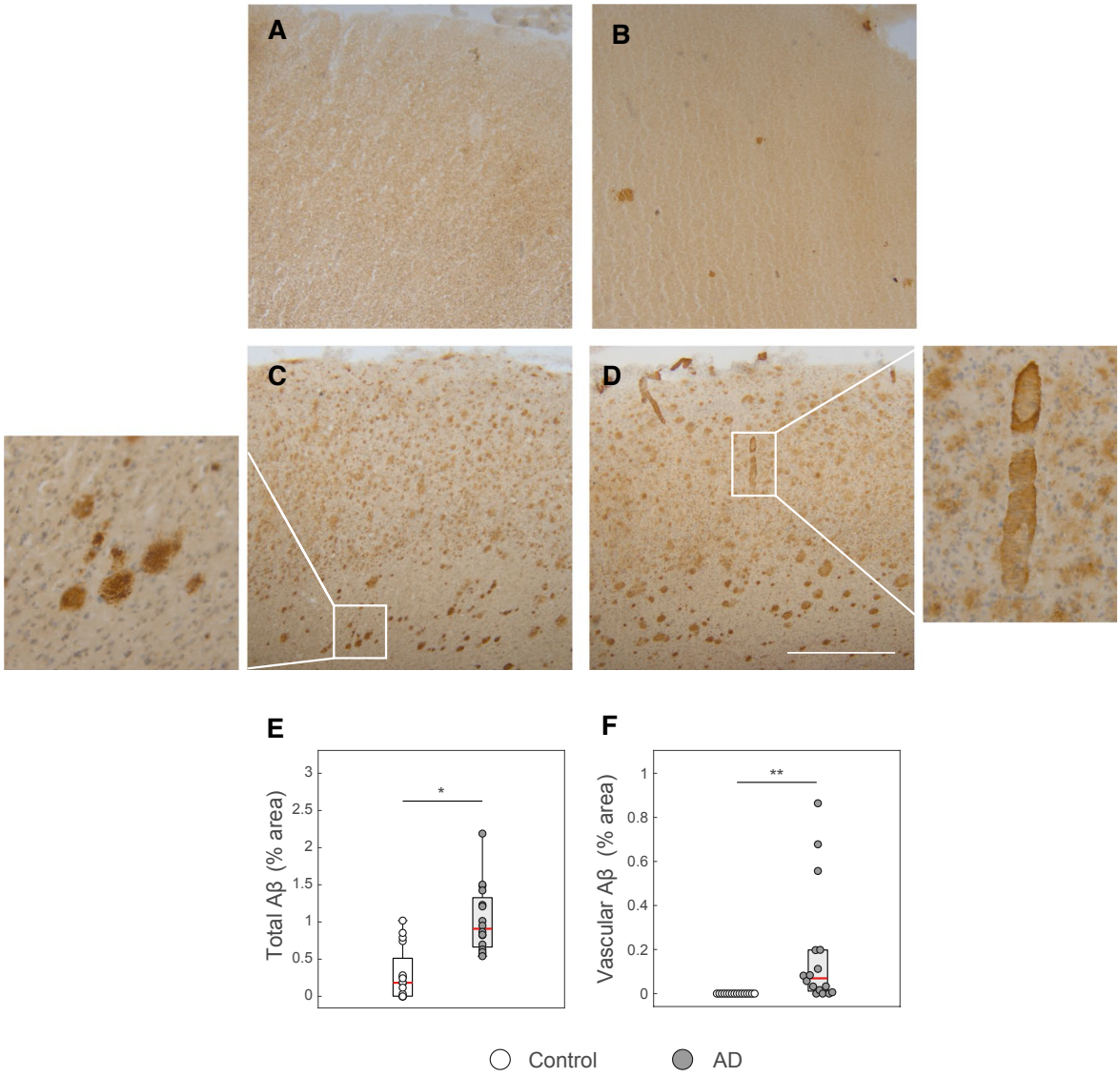

Figure 2. *Differences in Aβ between control and AD subjects*. **A-D.** Representative images of Aβ (brown) in control subjects (**A** and **B**) and AD subjects (**C** and **D**). The inset in **C** is an example of parenchymal Aβ. The inset in **D** is an example of vascular Aβ. **E.** Total Aβ was increased in AD pathology (* U = 27, z = -3.810, p = 0.0001; Mann-Whitney U test). **F.** Vascular Aβ was increased in AD pathology (** U = 24, z = -4.407, p < 0.0001; Mann-Whitney U test). Scale bar: 100 µm. Figure 2 is adapted from our publication[107].

In the AD cases, the score of neurofibrillary tangles (NFT) varied from mild (n = 3/16) over moderate (n = 10/16) to severe (n = 3/16; Table 1). AD subjects were characterized by moderate (n = 11/16) to frequent (n = 5/16) scores of neuritic plaques (CERAD[15]; Table 1). The degree of atrophy varied from mild (n = 7/16) over moderate (n = 5/16) to severe (n = 4/16) in AD cases (Table 1).

The APOE status was available for n = 16 control subjects and n = 10 AD subjects (Table 1): n = 3 control subjects and n = 4 AD subjects were homo- or heterozygous for the APOE4 allele, while n = 13 control subjects and n = 6 AD subjects presented with other combinations of the APOE2 and APOE3 alleles.

The dementia duration was determined for 9/16 cases and varied between 2-20 years (Table 1). The cause of death was unevenly distributed between AD and control, as respiratory infections (e.g. pneumonia) were predominant in AD and cardiovascular disease (e.g. myocardial infarct) was predominant in controls (Table 1).

3.2. Morphometric analyses

Tissue staining was homogeneous throughout the thickness of the section and the typical background signal in fresh frozen tissue did not interfere with distinction of structures (Figure 3). The strong signal from the basement membrane of the vasculature (laminin immunoreactivity) and pericytes (PDGFRβ immunoreactivity) enabled clear morphological identification of the structures (Figure 3).

In the multivariate analysis, we detected a difference in the combined microvascular morphometric measures (i.e. pericyte density, pericyte linear density, capillary density, intermediate vessel density, and large vessel density) between control and AD (control vs. AD; n = 16 vs. n = 16; $F_{5,26} = 4.400$, $p = 0.0049$, Wilks' $\Lambda = 0.542$, partial $\eta^2 = 0.458$; one-way MANOVA).

Follow-up univariate analyses (ANOVAs) were performed for each microvascular morphometric measure included in the multivariate analysis. The results of the univariate analyses are described in the following sections 3.2.1. and 3.2.2.

3.2.1. No pericyte loss in AD pathology

Compared to control cases, pericyte density (i.e. number of pericytes per tissue volume) was increased by 28% in AD cases (control vs. AD; 2412 ± 376 vs. 3081 ± 584 cells/mm^3; $F_{1,30} = 14.836$, $p = 0.0006$, partial $\eta^2 = 0.331$; one-way ANOVA; Figure 3).

The 28% increase in pericyte density was paralleled by a 24% increase in capillary density (Figure 4). Therefore, in the analysis of the primary outcome parameter, we detected no significant difference in pericyte linear density (i.e. number of pericytes per capillary length) between control and AD cases (control vs. AD; 8.3 ± 0.7 vs. 8.5 ± 1 cells/mm capillary; $F_{1,30} = 0.551$, $p = 0.4635$, partial $\eta^2 = 0.018$; one-way ANOVA; Figure 3).

Our results did not indicate a significant difference in pericyte coverage (i.e. percentage of capillary area covered by pericytes) between control and AD subjects (controls: median 75.6%, IQR 15; AD: median 75.8%, IQR 13.2; U = 120, z = -0.302, p = 0.7804; Mann-Whitney U test; Figure 3).

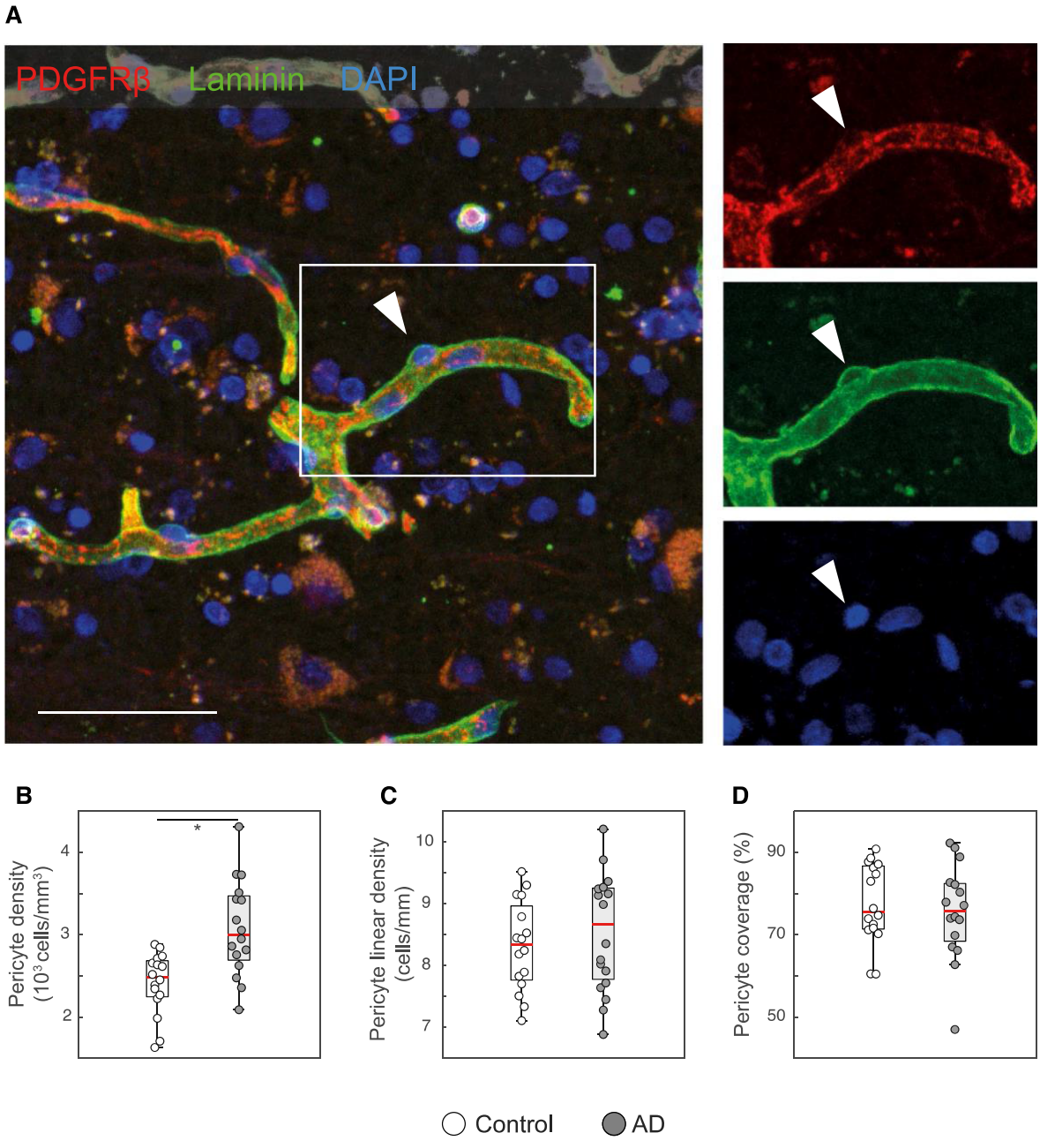

Figure 3. *Pericytes in AD pathology*. **A.** Representative confocal image of a pericyte (arrowhead). The PDGFRβ$^+$ pericyte is embedded within the laminin$^+$ basement membrane and contains a DAPI$^+$ nucleus. **B.** The pericyte density (number of pericytes per tissue volume) was increased in AD subjects (* $F_{1,30}$ = 14.836, p = 0.0006, partial η^2 = 0.331; one-way ANOVA). **C** and **D.** There was no significant difference in pericyte linear density (number of pericytes per capillary length) and pericyte coverage (percentage of capillary area covered by pericytes) between control and AD cases (statistical tests described in section 3.2.1.). Scale bar: 50 µm. Figure 3 is adapted from our publication[107].

Pericyte linear density showed no significant difference between AD subjects that were stratified by neuropathological and genetical characteristics (i.e. score/category of CERAD, NFTs, atrophy, APOE, and capillary CAA; Table 2).

Pericyte linear density and total Aβ showed only a weak correlation (control and AD, n = 32; $r_s = 0.0952$, $p = 0.6042$; Spearman's rank-order correlation).

Table 2. Pericyte linear density in AD subjects that were stratified by neuropathological and genetical measures.

Measure	Score/ Category	Number of AD cases	Median (IQR) pericyte linear density (cells/mm capillary)	Statistical test
CERAD	Moderate	11	8.4 (1.2)	U = 24, z = -0.397, p = 0.7427; Mann-Whitney U test
	Severe	5	9 (2)	
NFT	Mild	3	9.1 (1)	$\chi^2(2) = 0.224$, p = 0.8943; Kruskal-Wallis H test
	Moderate	10	8.2 (1.3)	
	Severe	3	9 (1.1)	
Atrophy	Mild	7	8 (1)	$\chi^2(2) = 1.238$, p = 0.5386; Kruskal-Wallis H test
	Moderate	5	9.1 (1.2)	
	Severe	4	9.2 (1)	
APOE	APOE2-3	6	7.8 (1.2)	U = 4, z = -1.706, p = 0.1143; Mann-Whitney U test
	APOE4	4	8.9 (1.2)	
Capillary CAA	Negative	13	9.7 (1.4)	U = 11, z = -1.144, p = 0.2964; Mann-Whitney U test
	Positive	3	8.4 (1.3)	

Abbreviations: AD, subject with Alzheimer's disease; APOE, apolipoprotein E; NFT, neurofibrillary tangles; CERAD, Consortium to Establish a Registry for Alzheimer's Disease[106]; CAA, cerebral amyloid angiopathy[62]; IQR, interquartile range. Subjects in the APOE4 subgroup were homo- or heterozygous for the APOE4 allele (Table 1).

3.2.2. Increase in vascular density is limited to capillaries in AD pathology

Compared to control cases, capillary density was increased by 24% in AD cases (control vs. AD; 291 ± 39 vs. 361 ± 48 mm/mm^3; $F_{1,30} = 20.851$, $p < 0.0001$, partial $\eta^2 = 0.410$; one-way ANOVA; Figure 4).

In AD subjects, the increase in vascular density was limited to capillaries. We did not detect a significant difference in intermediate and large vessels between control and AD cases: intermediate vessel density was 72 ± 23 mm/mm^3 in control subjects and 73 ± 27 mm/mm^3 in AD subjects ($F_{1,30} = 0.016$, $p = 0.9003$, partial $\eta^2 = 0.001$; one-way ANOVA; Figure 4). Large vessel density was 0.55 ± 0.25 mm/mm^3 in control subjects and 0.43 ± 0.30 mm/mm^3 in AD subjects ($F_{1,30} = 1.438$, $p = 0.2398$, partial $\eta^2 = 0.046$; one-way ANOVA; Figure 4).

In a post-hoc exploratory analysis, capillary density correlated strongly with total Aβ (AD and control, $n = 32$; $r_s = 0.6419$, $p < 0.0001$; Spearman's rank-order correlation; Figure 4).

In another post-hoc exploratory analysis, we determined the capillary density between the scores of atrophy: median capillary density was 349 mm/mm^3 (IQR 50) in subjects with mild atrophy, 325 mm/mm^3 (IQR 24) in subjects with moderate atrophy, and 407 mm/mm^3 (IQR 20) in subjects with severe atrophy ($\chi^2(2) = 5.893$, $p = 0.0525$; Kruskal-Wallis H test).

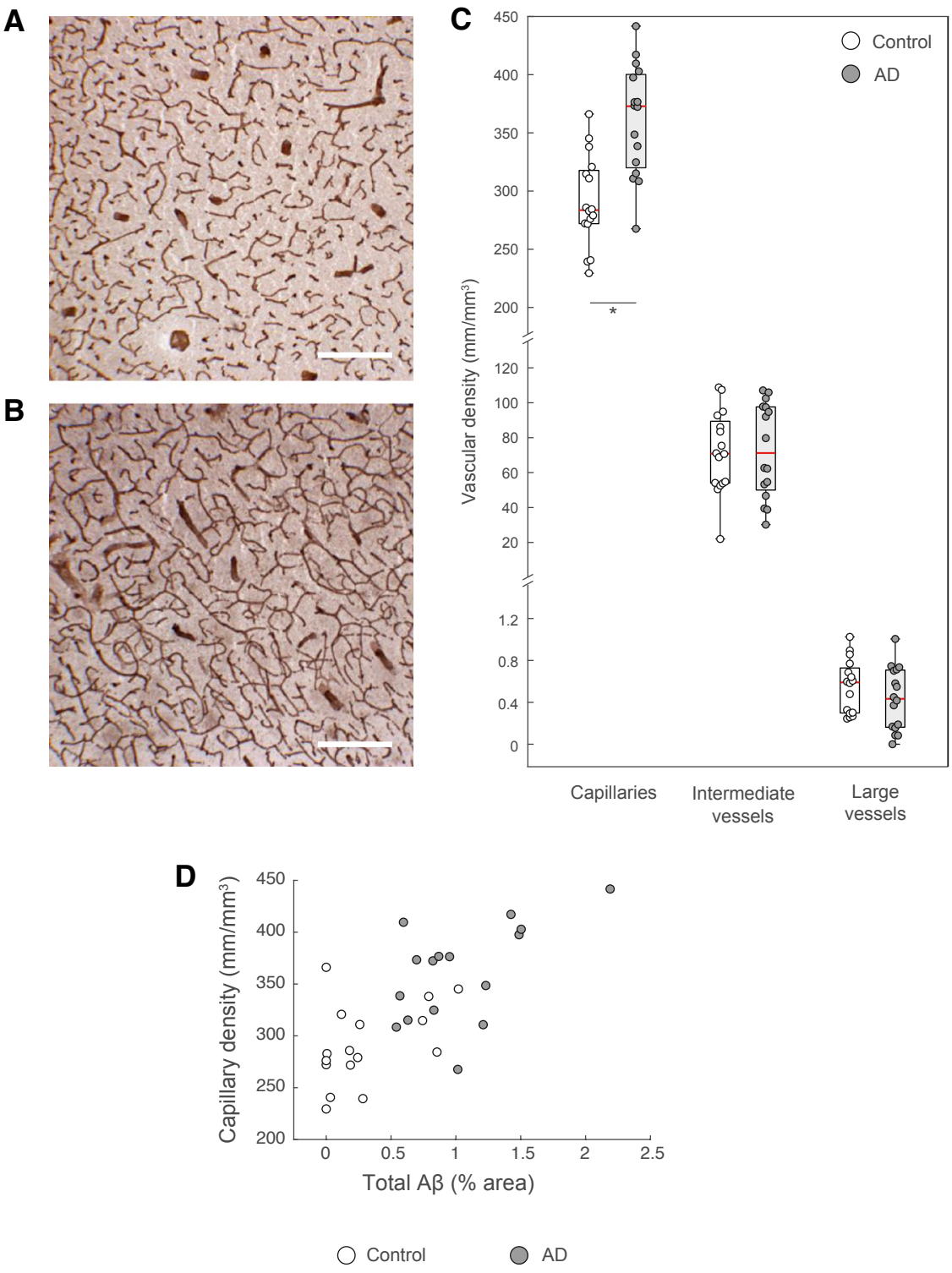

Figure 4. *Vascular density in AD pathology*. **A** and **B.** Representative images of the laminin^{+} (brown) vasculature in control subjects (**A**) and AD subjects (**B**). **C.** The capillary density was increased in AD cases (* $F_{1,30} = 20.851$, $p < 0.0001$, partial $\eta^2 = 0.410$; one-way ANOVA), while the intermediate vessel density and large vessel density were not significantly different between control and AD cases (statistical tests are described in section 3.2.2.). **D.** Capillary density correlated strongly with total Aβ ($r_s = 0.6419$, $p < 0.0001$; Spearman's rank-order correlation). Scale bars: 250 µm. Figure 4 is adapted from our publication[107].

3.2.3. Proliferating pericytes and endothelial cells

We investigated the proliferation of pericytes and endothelial cells and measured the number of Ki67-expressing cells in the capillary compartment of control and AD cases.

Tissue staining was homogeneous and the strong immunoreactivity from the basement membrane (laminin), the proliferation marker (Ki67), and DAPI facilitated the morphological distinction of structures (Figure 5).

Proliferating pericytes were rare events in both control and AD cases: in total, seven proliferating pericytes were detected in the control group and five proliferating pericytes were detected in the AD group (Figure 5). There was no significant difference between control (median 0 cells $\times 10^{-3}$ / mm, IQR 0.8) and AD (median 0 cells $\times 10^{-3}$ / mm, IQR 0) cases with regard to proliferating pericytes ($U = 96.5$, $z = -1.445$, $p = 0.2388$; Mann-Whitney U test; Figure 5).

There was no significant difference between control (median 0.33 cells $\times 10^{-2}$ / mm, IQR 0.55) and AD cases (median 0.15 cells $\times 10^{-2}$ / mm, IQR 0.29) with regard to proliferating endothelial cells ($U = 77$, $z = -1.932$, $p = 0.0562$; Mann-Whitney U test; Figure 5).

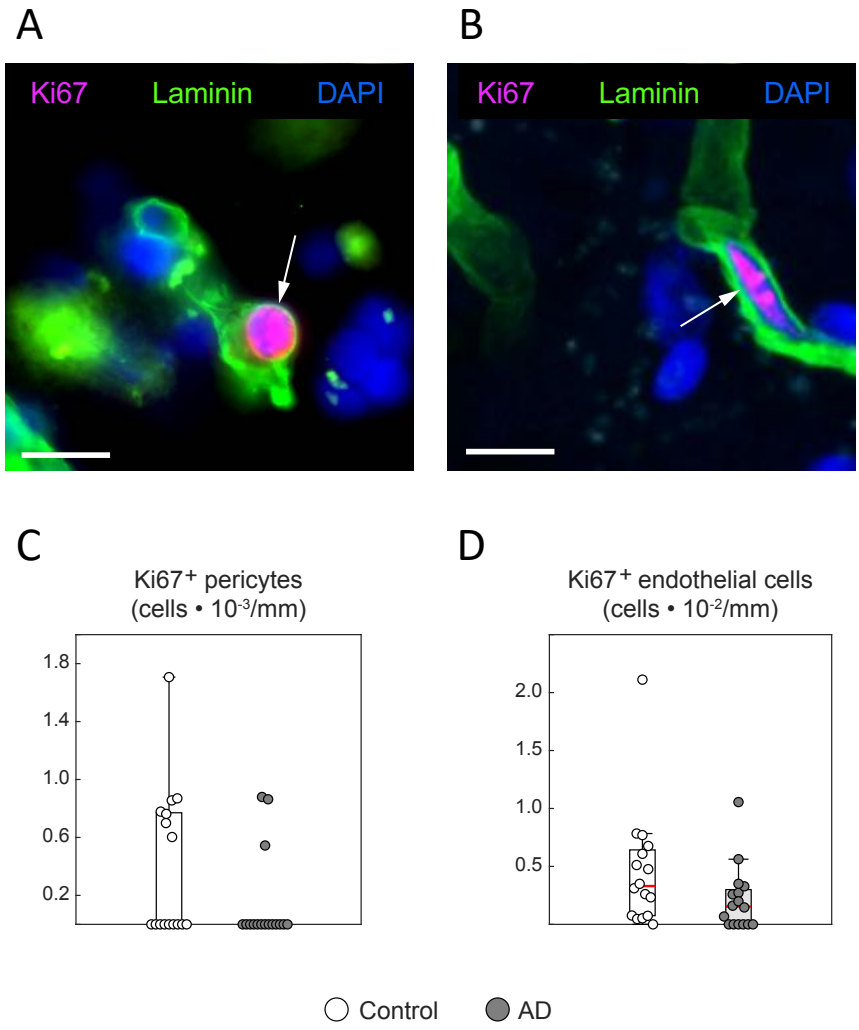

Figure 5. *Proliferating pericytes and endothelial cells in control and AD subjects*. **A** and **B.** Representative confocal images of a proliferating Ki67$^+$ pericyte (arrow, **A**) and a proliferating Ki67$^+$ endothelial cell (arrow, **B**). **C** and **D.** We detected no significant difference in proliferating Ki67$^+$ pericytes per capillary length (**C**) and proliferating Ki67$^+$ endothelial cells per capillary length (**D**) between control and AD cases. Scale bars: 10µm.

4. Discussion

4.1. Summary

This analysis yielded the following main results: contrary to our hypotheses (section 1.3.), we detected no evidence of pericyte loss in the middle frontal gyrus of subjects with AD pathology. We detected no significant difference in pericyte linear density (number of pericytes per capillary length) or pericyte coverage (area of capillaries covered by pericytes) in AD cases compared to the control cases.

Capillary density was increased in the AD group. The increase in capillary density (capillary length per tissue volume) was paralleled by an increase in pericyte density (number of pericytes per tissue volume), which indicates a quantitatively preserved pericyte population.

The increase in vascular density was limited to capillaries and did not include intermediate and large vessels. Total amyloid beta was increased in AD pathology and capillary density showed a strong positive correlation with total amyloid beta.

Proliferating pericytes and endothelial cells were rare events with no significant difference between AD and control cases.

In conclusion, we detected a dense capillary network with a quantitatively preserved pericyte population in AD pathology. Based on our findings, the differences in the microvascular network between control and AD cases are schematically illustrated in Figure 6. Possible limitations, explanations, and implications of these findings are discussed in the following sections.

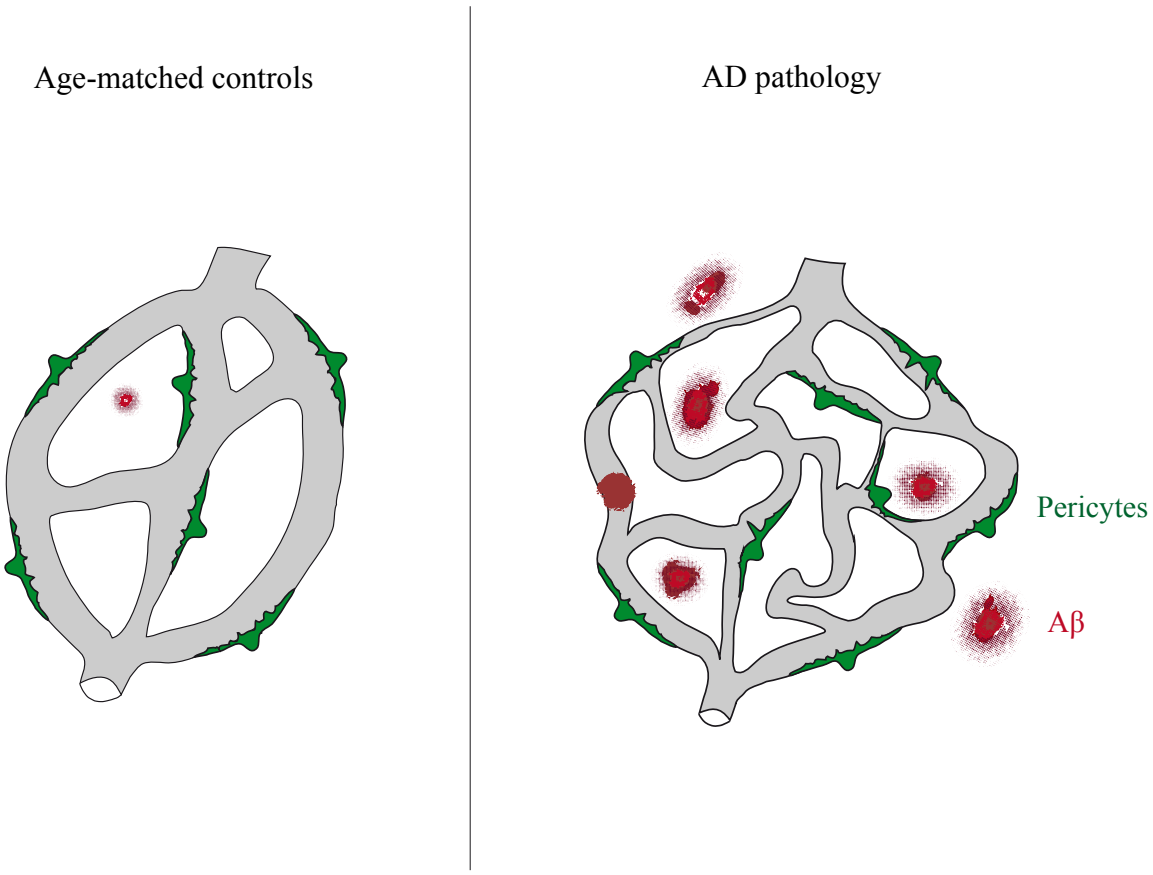

Figure 6. *Illustration of the main morphometric findings*. This schematic illustration depicts the main findings of our study: pericyte linear density (number of pericytes per capillary length) was not significantly different between AD and age-matched control cases. Capillary density and Aβ were increased in subjects with AD pathology. Accordingly, the illustration shows a dense capillary network with a quantitatively preserved pericyte population in AD pathology.

4.2. Limitations

First, we only analysed microvascular changes in the middle frontal gyrus. The inclusion of a single frontal region is a limitation of our study because other regions such as the hippocampus are typically affected earlier and more severely by AD pathology[121]. It could be hypothesized that the hippocampus shows more pronounced microvascular changes than samples of a frontal region. The inclusion of a single frontal region in this study limits generalizability of findings and further research is needed to investigate regional patterns of microvascular remodelling in AD pathology.

Nevertheless, reports from a series of other studies[41,43-45] – albeit not all other studies[50-52,59] – have shown relative increases in capillary density in frontal and temporal regions that are comparable to our results (discussed in section 4.3.2.). These findings suggest that

microvascular changes are not limited to temporal regions but also affect other regions such as the frontal cortex.

In addition, reports on pericyte quantification in AD pathology have not demonstrated a clear regional pattern: some studies reported no loss of pericytes in frontal, limbic, and other cortical regions[97,100,107] while other studies reported a loss in frontal and limbic regions[52,59,103]. Differences in methods between these studies may have contributed to the heterogenous findings of pericyte quantification (discussed in section 4.2.1).

Second, we implemented the neuropathological and genetical measures CERAD, NFT, atrophy, capillary CAA, vascular Aβ, total Aβ, and APOE to characterize subjects. Even though the implemented neuropathological and genetical measures cover several domains of AD pathology, more comprehensive scores such as the neuropathological score recommended in the National Institute on Aging–Alzheimer's Association guidelines[15], MRI assisted evaluation of atrophy, and detailed neuropsychological assessments of all subjects would have increased the validity of our results.

Third, a proportion of the tissue samples in the control group showed Aβ immunoreactivity (median 0.18% of the tissue area). Aβ deposition has been reported in elderly persons without dementia[17,122] but future studies may reduce potential confounding associated with amyloid pathology by including control subjects without Aβ deposition.

Fourth, even though this study to our knowledge includes one of the largest samples (N = 32) in the investigation of pericyte linear density in AD pathology, and we calculated a sample size estimate for the main analysis (MANOVA), smaller differences between groups were possibly not detected. The risk of false negative findings is particularly increased in analyses with rare secondary outcomes (e.g. proliferating endothelial cells and pericytes) that were not included in the sample size estimate.

Fifth, this was an exploratory study with an unadjusted alpha level, which increases the risk of false positive findings[119,149]. Based on our exploratory findings, a study with a confirmatory design[119,149] that is associated with less risk of false positive findings would be applicable to confirm or reject hypotheses, which were generated by this study.

Sixth, the risk of bias was augmented in the exploratory analyses with missing data, which were conducted with observed data only[150]: APOE status was missing for 6 out of 16 AD subjects due to insufficient material quantity. Only AD subjects had records of CERAD, NFTs, and atrophy because these parameters were not routinely assessed for the control subjects. According to the recommendations by Little et al. (2012)[150], rigorous study planning with the

aim to limit missing data (e.g. identical neuropathological assessment protocols for AD and control subjects) and predefined imputation strategies would further reduce the risk of bias in future studies.

Seventh, the samples examined in this study were matched with regard to sample size, age, and sex. However, the cause of death was asymmetrical between subjects. AD cases died more frequently of respiratory infections such as pneumonia while controls died more frequently of cardiovascular disease such as myocardial infarct. This asymmetry has also been reported in other human AD post-mortem studies[41,56] and may be due to the increased risk of aspiration in dementia. Respiratory system disease (e.g. pneumonia) is a common comorbidity and cause of death in AD[125]. It cannot be ruled out that a mismatch in cause of death has an impact on CNS microvascular findings: for instance, accentuated microvascular remodelling in control subjects with cardiovascular disease could hypothetically contribute to an underestimate of microvascular remodelling in subjects with AD[29,32].

Eighth, the PDGFRβ antibody could not be included in the Ki67 staining due to technical restrictions in the staining procedure (i.e. limited possible combinations of first and secondary antibodies; section 2.2.1.). Only Ki67, laminin, and DAPI were included in this staining and cells were distinguished based on morphology and location. PDGFRβ immunoreactivity supports identification of pericytes and the lack of the PDGFRβ antibody in this staining is a source of potential confounding.

Ninth, we investigated a limited sample of middle frontal gyrus specimens and acquired density outcomes. We did not acquire total number/length outcomes. Densities are commonly used to make relative comparisons between groups[41], but systematic random sampling of a complete brain region that results in total numbers/lengths instead of densities is considered to be more accurate[50,110]. Provided that a complete brain region is available, estimating the total number of pericytes and total length of capillaries would contribute to a more comprehensive understanding of microvascular morphometry in AD pathology.

Tenth, the spaceballs method is a well-established stereological method to determine capillary density[110]. Analyses of larger vessels with the spaceballs method have, to our knowledge, not previously been published, which may be due to the fact that analysis of less frequent events such as arterioles is very time-consuming with the regular approach (e.g. systematic random sampling of a large region of interest). The novel approach implemented in this study of sampling larger vessels only within smaller preselected regions of interest reduces sampling in spaces without larger vessels (section 2.3.4.). With this approach, sampling

efficiency is increased for less frequent events. However, systematic error may potentially arise from measuring vessels with large diameters as the location of the central axis of the vessel becomes more difficult to determine accurately[110]. Implementation of thicker tissue sections (if possible with regard to staining procedures) may help to identify the central axis of the vessel and reduce the risk of systematic error[110].

4.3. Microvascular morphometry in AD pathology

4.3.1. Pericyte morphometry in AD pathology

Pericyte degeneration and loss have been suggested to be early events in the development of AD pathology[26,59,103]. However, our assessment did not show evidence of pericyte loss in AD pathology since we detected no difference in pericyte linear density between AD and control cases (Figure 3). Furthermore, we detected no difference in pericyte linear density between subjects with different scores/categories of neuropathological and genetical measures such as CERAD, NFTs, atrophy, APOE status, and capillary CAA. Pericyte linear density only showed a weak correlation with total Aβ. Consistently, we detected no significant difference in pericyte coverage between AD and control subjects.

Findings in the literature are heterogeneous: the density of pericytes on capillaries (e.g. pericyte linear density) varied from unchanged[97,100] to decreased[52,59,103] in AD pathology. An even greater variance in findings was reported for the area of capillaries covered by pericytes (e.g. pericyte coverage): these findings varied from decreased[59,103], to unchanged[51,107] or increased[100] area of capillaries covered by pericytes in AD pathology .

Differences in methods, in particular the choice of pericyte markers and techniques of measuring pericyte densities, may have contributed to the discrepancies in the literature. We combined a molecular and a morphological marker to identify pericytes during the stereological analysis of the primary outcome measure pericyte linear density (pericyte cells / mm capillary). Other image analysis methods[59] that focus on the intensity threshold of the immunofluorescence signal and estimates of pericyte numbers per vascular area (pericyte cells / mm^2 capillary) may be more sensitive to changes in the intensity of the fluorescence signal in pericytes and capillaries. Changes in the intensity of the fluorescence signal from microvascular components could occur in AD pathology due to altered expression of microvascular proteins: for example, in vitro studies with pericytes suggested that Aβ and hypoxia may induce shedding of the protein PDGFRβ (i.e. loss of pericyte cell-associated PDGFRβ)[126,127]. It appears possible that

shedding of PDGFRβ could result in a reduced intensity of the pericyte cell-associated PDGFRβ fluorescence signal in AD pathology. On the other hand, Ulex europeaus agglutinin I has been used to identify the vasculature[103] and this marker may not show a reduced intensity of the fluorescence signal in AD pathology: ulex europeaus agglutinin I binds to fucosylated glycoproteins that are associated with leucocyte adhesion and endothelial activation[128]. Leucocyte adhesion and endothelial activation increase in AD pathology, which could potentially amplify the ulex europeaus agglutinin I signal[129]. In summary, a decreased PDGFRβ signal in combination with an unchanged or increased ulex europeaus agglutinin I signal may more likely suggest pericyte loss if the quantification method is sensitive to changes in the fluorescence signal. Altered patterns of protein expression and differences in morphometrical methods could have contributed to the heterogeneous findings of pericyte morphometry between studies.

We detected no significant difference in pericyte linear density in AD pathology, but importantly, unaltered pericyte functions cannot be concluded from these morphometrical findings. As mentioned in the introduction (section 1.2.), pericyte dysfunction has been suggested via different pathways in AD pathology (e.g. deficient signal transduction via the PDGF-BB–PDGFRβ pathway[67]). Aβ deposition may have an impact on pericyte function with regard to regulation of cerebral blood flow since Aβ recently has been reported to constrict capillaries at pericyte locations[130]: pericyte constriction could result from Aβ induced reactive oxygen species, which cause the release of the vasoconstrictive endothelin-1 (ET) and subsequent binding of ET to ET_A receptors on pericytes[130].

In addition, Aβ deposition in vessels induces inflammatory processes and pericytes participate in these processes via production of immunomodulating cytokines and chemokines[131].

In conclusion, we detected no evidence of pericyte loss in AD pathology and further research is needed to elucidate the functional role of pericytes for the development of AD pathology. Emerging techniques that further uncover molecular characteristics of mural cells in the cerebral vasculature[132] may provide insights for future research on pericytes in AD pathology.

4.3.2. Capillary morphometry in AD pathology

We detected a 24% increase in capillary density in the frontal cortex of AD subjects. These findings are in line with two other studies that implemented the same stereological method (spaceballs): Schwartz et al. (2010) showed an increase in capillary density in the hippocampus

of AD cases[46] and Richard et al. (2010) reported a 33% increase in capillary density in the temporal cortex of samples with AD pathology[41].

A range of morphometric methods (e.g. test grids[44,53,56,57] or threshold techniques[51,54]) were previously implemented to assess microvascular density in AD pathology and results ranged from increased[39-46,107] to unchanged[47-52] or decreased[53-60] microvascular density. Differences between studies may be influenced by methodological factors such as differences in microvascular definitions: some studies, for example, did not exclude vessels larger than capillaries or did not report the use vascular diameters to define capillaries[39,40,42,48,49,51,54,55,57,58]. Pooling data from capillaries and vessels larger than capillaries could affect results since the different vascular segments may not show identical density changes. In addition to differences in demographic and neuropathological characteristics between studies, a number of studies included only small AD sample sizes of ≤5 cases[43,54-56], which may also have contributed to the heterogeneity of findings between studies.

In our study, vessels larger than capillaries did not change significantly in density. This finding complements the sparse morphometric literature on arteriolar density in AD pathology: in 1981, Bell et al. investigated a small subgroup of arterioles (diameter 10-30µm) and reported an increase in arteriolar density in the hippocampus of AD subjects[43]. At that time, however, they used a tracing digitizer method sensitive to volume loss. Five years later, the same authors investigated overall change in microvascular length (capillaries and arterioles combined) in the hippocampus and calcarine cortex[133] and detected no significant change in either of these areas. In another study in 1990, the same authors found no difference in arteriolar density between AD and control cases in the visual cortex[47].

Overall, findings suggest that mainly the capillary segment of microvascular network increases in density in AD pathology. The evidence that capillary density is increased in AD pathology could be further assessed in a future systematic review and meta-analysis that includes a comprehensive synthesis and evaluation of data from previous studies.

4.3.3. Interpretation of increased capillary density with preserved pericytes in AD pathology

We detected an increase in capillary density without pericyte loss in the middle frontal gyrus of AD cases. Increased capillary density may be interpreted as the result of angiogenesis[134]. However, the interpretation of increased capillary density requires consideration of parenchymal volume loss (e.g. due to cortical atrophy)[41].

Theoretically, volume loss affects all segments of the vascular network, which may contribute to an increase in vascular density in all segments. In this study, the increase in vessel density was restricted to the capillary segment. This finding argues against parenchymal volume loss as the only cause for the increased capillary density in the AD cases.

In our post-hoc analysis, the difference in capillary density between subjects that were stratified according to the atrophy score was not significant but this analysis was limited by small sample sizes. In addition, only a four-tier measure of atrophy was available, which lacked the accuracy of a more detailed assessment of regional atrophy. Lastly, parenchymal volume loss and angiogenesis may not necessarily be mutually exclusive and could hypothetically both contribute to increased capillary density in AD pathology.

The mitotic Ki67 proliferation marker showed no significant difference between control and AD cases. Since $Ki67^{+}$ vascular cells were rare events, this study may not have had sufficient statistical power to detect differences in the proliferation marker between groups. Albeit speculative, vascular cell proliferation might peak early in the development of AD pathology since angiogenic stimuli such as hypoxia are assumed to emerge in the early stages of the disease development[33]. This could be another possible explanation why we detected increased capillary density but did not detect increased vascular cell proliferation in subjects with established AD pathology.

Our findings of increased capillary density are in agreement with upregulated angiogenesis-related gene expression in transgenic mice models of AD pathology and human AD pathology[135,136]. Recently, the angiogenic factor angiopoietin like-4 (ANGPTL4)[137] has been suggested to contribute to vascular remodelling in capillary CAA. Increased levels of other angiogenic factors such as vascular endothelial growth factor (VEGF) were indicated in several[127,138-141], but not all[142,143], studies with human samples of AD pathology. Insufficient cerebral perfusion and increased inflammation may amplify angiogenesis in AD pathology but the exact mechanisms remain to be fully determined[21,129,144-148].

In conclusion, angiogenesis appears to contribute to increased capillary density in AD pathology. Further research is needed to differentiate between the effects of angiogenesis and parenchymal volume loss on capillary density in AD pathology.

References

1 Arvanitakis Z, Shah RC, Bennett DA. Diagnosis and Management of Dementia: Review. *JAMA* 2019; **322**: 1589–11.

2 Bacigalupo I, Mayer F, Lacorte E, Di Pucchio A, Marzolini F, Canevelli M, Di Fiandra T, Vanacore N. A Systematic Review and Meta-Analysis on the Prevalence of Dementia in Europe: Estimates from the Highest-Quality Studies Adopting the DSM IV Diagnostic Criteria. *J Alzheimers Dis* 2018; **66**: 1471–81.

3 Barnes D, Yaffe K. The projected effect of risk factor reduction on Alzheimer's disease prevalence. *Lancet Neurol* 2011; **10**: 819–28.

4 Prince M, Albanese E, Guerchet M, Prina M. World Alzheimer Report 2014 – Dementia and Risk Reduction: an analysis of protective and modifiable risk factors. London, United Kingdom: Alzheimers Disease International, 2014.

5 Bickel H. Die Häufigkeit von Demenzerkrankungen. Berlin, Germany: Deutsche Alzheimer Gesellschaft, 2020.

6 Alzheimer's Disease International. World Alzheimer Report 2019: attitudes to dementia. London, United Kingdom: Alzheimer's Disease International, 2019.

7 Alzheimer Europe. Dementia in Europe Yearbook 2019. Luxembourg City, Luxembourg: Alzheimer Europe, 2020.

8 Alzheimer's Disease International. World Alzheimer Report 2015 – The Global Impact of Dementia: an analysis of prevalence, incidence, cost and trends. London, United Kingdom: Alzheimer's Disease International, 2015.

9 The Alzheimer's Association. 2020 Alzheimer's disease facts and figures. *Alzheimers Dement* 2020; **16**: 391–460.

10 Xu J, Murphy S, Kochanek K, Arias E. Mortality in the United States, 2018. NCHS Data Brief; No. 355. Hyattsville, MD, USA: National Center for Health Statistics, 2020.

11 GBD 2015 Mortality and Causes of Death Collaborators. Global, regional, and national life expectancy, all-cause mortality, and cause-specific mortality for 249 causes of death, 1980–2015: a systematic analysis for the Global Burden of Disease Study 2015. *Lancet* 2016; **388**: 1459–544.

12 Dubois B, Feldman HH, Jacova C, Cummings JL, DeKosky ST, Barberger-Gateau P, Delacourte A, Frisoni G, Fox NC, Galasko D, Gauthier S, Hampel H, Jicha GA, Meguro K, O'Brien J, Pasquier F, Robert P, Rossor M, Salloway S, Sarazin M, de Souza LC, Stern Y, Visser PJ, Scheltens P. Revising the definition of Alzheimer's disease: a new lexicon. *Lancet Neurol* 2010; **9**: 1118–27.

13 American Psychiatric Association. Diagnostic and statistical manual of mental disorders, 5th edn. Arlington, VA, USA: American Psychiatric Association, 2013.

14 World Health Organization. ICD-10: international statistical classification of diseases and related health problems: tenth revision, 2nd edn. Geneva, Switzerland: World Health Organization, 2004.

15 Montine TJ, Phelps CH, Beach TG, Bigio EH, Cairns NJ, Dickson DW, Duyckaerts C, Frosch MP, Masliah E, Mirra SS, Nelson PT, Schneider JA, Thal DR, Trojanowski JQ, Vinters HV, Hyman B. National Institute on Aging–Alzheimer‘s Association guidelines for the neuropathologic assessment of Alzheimer’s disease: a practical approach. Acta Neuropathol. 2012; **123**: 1–11.

16 Alzheimer A. Über einen eigenartigen, schweren Erkrankungsprozeß der Hirnrinde. *Neurologisches Centralblatt* 1906; **23**: 1129–36.

17 Glenner GG, Wong CW. Alzheimer's disease: initial report of the purification and characterization of a novel cerebrovascular amyloid protein. *Biochem Biophys Res Commun* 1984; **120**: 885–90.

18 Glenner GG, Wong CW. Alzheimer‘s disease and Down’s syndrome: sharing of a unique cerebrovascular amyloid fibril protein. *Biochem Biophys Res Commun* 1984; **122**: 1131–5.

19 Bennett DA, Schneider JA, Arvanitakis Z, Kelly JF, Aggarwal NT, Shah RC, Wilson RS. Neuropathology of older persons without cognitive impairment from two community-based studies. *Neurology* 2006; **66**: 1837–44.

20 Coulson EJ, Paliga K, Beyreuther K, Masters CL. What the evolution of the amyloid protein precursor supergene family tells us about its function. *Neurochem Int* 2000; **36**: 175–84.

21 Ethell DW. An amyloid-notch hypothesis for Alzheimer's disease. *Neuroscientist* 2010; **16**: 614–7.

22 Hamley IW. The amyloid beta peptide: a chemist’s perspective. Role in Alzheimer’s and fibrillization. *Chem Rev* 2012; **112**: 5147–92.

23 Selkoe DJ, Hardy J. The amyloid hypothesis of Alzheimer's disease at 25 years. *EMBO Mol Med* 2016; **8**: 595–608.

24 Tanzi RE. The Genetics of Alzheimer Disease. *Cold Spring Harb Perspect Med* 2012; **2**: a006296.

25 Baranello RJ, Bharani KL, Padmaraju V, Chopra N, Lahiri DK, Greig NH, Pappolla MA, Sambamurti K. Amyloid-Beta Protein Clearance and Degradation (ABCD) Pathways and their Role in Alzheimer's Disease. *Curr Alzheimer Res* 2015; **12**: 32–46.

26 Kisler K, Nelson AR, Montagne A, Zlokovic BV. Cerebral blood flow regulation and neurovascular dysfunction in Alzheimer disease. *Nature* 2017; **18**: 419–34.

27 la Torre de JC. Alzheimer's disease is a vasocognopathy: a new term to describe its nature. *Neurol Res* 2004; **26**: 517–24.

28 Zlokovic BV. Neurovascular pathways to neurodegeneration in Alzheimer's disease and other disorders. *Nat Rev Neurosci* 2011; **12**: 723–38.

29 Ostergaard L, Aamand R, Gutiérrez-Jiménez E, Ho YCL, Blicher JU, Madsen SM, Nagenthiraja K, Dalby RB, Drasbek KR, Møller A, Brændgaard H, Mouridsen K, Jespersen SN, Jensen MS, West MJ. The capillary dysfunction hypothesis of Alzheimer's disease. *Neurobiol Aging* 2013; **34**: 1018–31.

30 Zlokovic BV. Neurovascular mechanisms of Alzheimer's neurodegeneration. *Trends Neurosci* 2005; **28**: 202–8.

31 la Torre de JC. Critically Attained Threshold of Cerebral Hypoperfusion: Can It Cause Alzheimer's Disease? *Ann N Y Acad Sci* 2000; **903**: 424–36.

32 Baumgart M, Snyder HM, Carrillo MC, Fazio S, Kim H, Johns H. Summary of the evidence on modifiable risk factors for cognitive decline and dementia: A population-based perspective. *Alzheimers Dement* 2015; **11**: 718–26.

33 Stone J. What initiates the formation of senile plaques? The origin of Alzheimer-like dementias in capillary haemorrhages. *Med Hypotheses* 2008; **71**: 347–59.

34 Zhang X, Le W. Pathological role of hypoxia in Alzheimer's disease. *Exp Neurol* 2010; **223**: 299–303.

35 Snowdon DA, Greiner LH, Mortimer JA, Riley KP, Greiner PA, Markesbery WR. Brain Infarction and the Clinical Expression of Alzheimer Disease. The Nun Study. *JAMA* 1997; **277**: 813–7.

36 Kalaria RN. Cerebral Vessels in Ageing and Alzheimer's Disease. *Pharmacol Ther* 1996; **72**: 193–214.

37 Baloyannis SJ, Baloyannis IS. The vascular factor in Alzheimer's disease: A study in Golgi technique and electron microscopy. *J Neurol Sci* 2012; **322**: 117–21.

38 Mendes-Jorge L, Llombart C, Ramos D, López-Luppo M, Valença A, Nacher V, Navarro M, Carretero A, Méndez-Ferrer S, Rodriguez-Baeza A, Ruberte J. Intercapillary bridging cells: Immunocytochemical characteristics of cells that connect blood vessels in the retina. *Exp Eye Res* 2012; **98**: 79–87.

39 Biron KE, Dickstein DL, Gopaul R, Jefferies WA. Amyloid Triggers Extensive Cerebral Angiogenesis Causing Blood Brain Barrier Permeability and Hypervascularity in Alzheimer's Disease. *PLoS ONE* 2011; **6**: e23789.

40 Jantaratnotai N, Schwab C, Ryu JK, McGeer PL, McLarnon JG. Converging perturbed microvasculature and microglial clusters characterize Alzheimer disease brain. *Curr Alzheimer Res* 2010; **7**: 625–36.

41 Richard E, van Gool WA, Hoozemans JJM, van Haastert ES, Eikelenboom P, Rozemuller AJM, van de Berg WDJ. Morphometric Changes in the Cortical Microvascular Network in Alzheimer's Disease. *J Alzheimers Dis* 2010; **22**: 811–8.

42 Desai BS, Schneider JA, Li J-L, Carvey PM, Hendey B. Evidence of angiogenic vessels in Alzheimer's disease. *J Neural Transm* 2009; **116**: 587–97.

43 Bell MA, Ball MJ. Morphometric comparison of hippocampal microvasculature in ageing and demented people: diameters and densities. *Acta Neuropathol* 1981; **53**: 299–318.

44 Meier-Ruge W, Ulrich J, Stähelin HB. Morphometric investigation of nerve cells, neuropil and senile plaques in senile dementia of the Alzheimer type. *Arch Gerontol Geriatr* 1985; **4**: 219–29.

45 Burke MJC, Nelson L, Slade JY, Oakley AE, Khundakar AA, Kalaria RN. Morphometry of the hippocampal microvasculature in post-stroke and age-related dementias. *Neuropathol Appl Neurobiol* 2014; **40**: 284–95.

46 Schwartz E, Wicinski B, Schmeidler J, Haroutunian V, Hof PR. Cardiovascular risk factors affect hippocampal microvasculature in early AD. *Transl Neurosci* 2010; **1**: 292–9.

47 Bell MA, Ball MJ. Neuritic plaques and vessels of visual cortex in aging and Alzheimer's dementia. *Neurobiol Aging* 1990; **11**: 359–70.

48 Hunter JM, Kwan J, Malek-Ahmadi M, Maarouf CL, Kokjohn TA, Belden C, Sabbagh MN, Beach TG, Roher AE. Morphological and Pathological Evolution of the Brain Microcirculation in Aging and Alzheimer's Disease. *PLoS ONE* 2012; **7**: e36893.

49 Challa VR, Thore CR, Moody DM, Anstrom JA, Brown WR. Increase of white matter string vessels in Alzheimer's disease. *J Alzheimers Dis* 2004; **6**: 379–83.

50 Bouras C, Kövari E, Herrmann FR, Rivara CB, Bailey TL, von Gunten A, Hof PR, Giannakopoulos P. Stereologic Analysis of Microvascular Morphology in the Elderly: Alzheimer Disease Pathology and Cognitive Status. *J Neuropathol Exp Neurol* 2006; **65**: 235–44.

51 Uemura MT, Ihara M, Maki T, Nakagomi T, Kaji S, Uemura K, Matsuyama T, Kalaria RN, Kinoshita A, Takahashi R. Pericyte-derived bone morphogenetic protein 4 underlies white matter damage after chronic hypoperfusion. *Brain Pathol* 2017; **95**: 78–15.

52 Schultz N, Brännström K, Byman E, Moussaud S, Nielsen HM, The Netherlands Brain Bank, Olofsson A, Wennström M. Amyloid-beta 1-40 is associated with alterations in NG2+ pericyte population ex vivo and in vitro. *Aging Cell* 2018; **17**: e12728.

53 Fischer VW, Siddiqi A, Yusufaly Y. Altered angioarchitecture in selected areas of brains with Alzheimer's disease. *Acta Neuropathol* 1990; **79**: 672–9.

54 Buée L, Hof PR, Bouras C, Delacourte A, Perl DP, Morrison JH, Fillit HM. Pathological alterations of the cerebral microvasculature in Alzheimer's disease and related dementing disorders. *Acta Neuropathol* 1994; **87**: 469–80.

55 Suter O-C, Sunthorn T, Kraftsik R, Straubel J, Darekar P, Khalili K, Miklossy J. Cerebral hypoperfusion generates cortical watershed microinfarcts in Alzheimer disease. *Stroke* 2002; **33**: 1986–92.

56 Mann DM, Eaves NR, Marcyniuk B, Yates PO. Quantitative changes in cerebral cortical microvasculature in ageing and dementia. *Neurobiol Aging* 1986; **7**: 321–30.

57 Kitaguchi H, Ihara M, Saiki H, Takahashi R, Tomimoto H. Capillary beds are decreased in Alzheimer‘s disease, but not in Binswanger's disease. *Neurosci Lett* 2007; **417**: 128–31.

58 Religa P, Cao R, Religa D, Xue Y, Bogdanovic N, Westaway D, Marti HH, Winblad B, Cao Y. VEGF significantly restores impaired memory behavior in Alzheimer's mice by improvement of vascular survival. *Sci Rep* 2013; **3**: 2053.

59 Halliday MR, Rege SV, Ma Q, Zhao Z, Miller CA, Winkler EA, Zlokovic BV. Accelerated pericyte degeneration and blood–brain barrier breakdown in apolipoprotein E4 carriers with Alzheimer's disease. *J Cereb Blood Flow Metab* 2016; **36**: 216–27.

60 Hase Y, Ding R, Harrison G, Hawthorne E, King A, Gettings S, Platten C, Stevenson W, Craggs LJL, Kalaria RN. White matter capillaries in vascular and neurodegenerative dementias. *Acta Neuropathol Commun* 2019; **7**: 16.

61 Thal DR, Griffin WST, de Vos RAI, Ghebremedhin E. Cerebral amyloid angiopathy and its relationship to Alzheimer's disease. *Acta Neuropathol* 2008; **115**: 599–609.

62 Thal DR, Ghebremedhin E, Orantes M, Wiestler OD. Vascular Pathology in Alzheimer Disease: Correlation of Cerebral Amyloid Angiopathy and Arteriosclerosis/Lipohyalinosis with Cognitive Decline. *J Neuropathol Exp Neurol* 2003; **62**: 1287–301.

63 Attems J, Jellinger KA. Only cerebral capillary amyloid angiopathy correlates with Alzheimer pathology – a pilot study. *Acta Neuropathol* 2004; **107**: 83–90.

64 Verbeek MM, de Waal RM, Schipper JJ, Van Nostrand WE. Rapid Degeneration of Cultured Human Brain Pericytes by Amyloid beta Protein. *J Neurochem* 1997; **68**: 1135–41.

65 Hamilton NB, Attwell D, Hall CN. Pericyte-mediated regulation of capillary diameter: a component of neurovascular coupling in health and disease. *Front Neuroenerg* 2010; **2**: 5.

66 Armulik A, Genové G, Betsholtz C. Pericytes: Developmental, Physiological, and Pathological Perspectives, Problems, and Promises. *Dev Cell* 2011; **21**: 193–215.

67 Sweeney MD, Ayyadurai S, Zlokovic BV. Pericytes of the neurovascular unit: key functions and signaling pathways. *Nat Neurosci* 2016; **19**: 771–83.

68 Eberth CJ. Von den Blutgefässen. In: Stricker S, ed. Handbuch der Lehre von den Geweben des Menschen und der Thiere. Leipzig, Germany: Engelmann, 1871.

69 Rouget C. Mémoire sur le développement, la structure et les propriétés physiologique des cappilaires sanguins et lymphatiques. *Archs Physiol Norm Pathol* 1873; **5**: 603–63.

70 Zimmermann KW. Der feinere Bau der Blutcapillaren. *Anat Embryol* 1923; **68**: 29–109.

71 Hartmann DA, Underly RG, Grant RI, Watson AN, Lindner V, Shih AY. Pericyte structure and distribution in the cerebral cortex revealed by high-resolution imaging of transgenic mice. *Neurophoton* 2015; **2**: 041402.

72 Mathiisen TM, Lehre KP, Danbolt NC, Ottersen OP. The Perivascular Astroglial Sheath Provides a Complete Covering of the Brain Microvessels: An Electron Microscopic 3D Reconstruction. *Glia* 2010; **58**: 1094–103.

73 Armulik A, Abramsson A, Betsholtz C. Endothelial/Pericyte Interactions. *Circ Res* 2005; **97**: 512–23.

74 Shepro D, Morel NM. Pericyte physiology. *FASEB J* 1993; **7**: 1031–8.

75 Storkebaum E, Quaegebeur A, Vikkula M, Carmeliet P. Cerebrovascular disorders: molecular insights and therapeutic opportunities. *Nat Neurosci* 2011; **14**: 1390–7.

76 Daneman R, Zhou L, Kebede AA, Barres BA. Pericytes are required for blood-brain barrier integrity during embryogenesis. *Nature* 2010; **468**: 562–6.

77 Holm A, Heumann T, Augustin HG. Microvascular Mural Cell Organotypic Heterogeneity and Functional Plasticity. *Trends in Cell Biology* 2018; **28**: 302–16.

78 Bandopadhyay R, Orte C, Lawrenson JG, Reid AR, De Silva S, Allt G. Contractile proteins in pericytes at the blood-brain and blood-retinal barriers. *J Neurocytol* 2001; **30**: 35–44.

79 Nakagomi T, Kubo S, Nakano-Doi A, Sakuma R, Lu S, Narita A, Kawahara M, Taguchi A, Matsuyama T. Brain Vascular Pericytes Following Ischemia Have Multipotential Stem Cell Activity to Differentiate Into Neural and Vascular Lineage Cells. *Stem Cells* 2015; **33**: 1962–74.

80 Guimarães-Camboa N, Cattaneo P, Sun Y, Moore-Morris T, Gu Y, Dalton ND, Rockenstein E, Masliah E, Peterson KL, Stallcup WB, Chen J, Evans SM. Pericytes of Multiple Organs Do Not Behave as Mesenchymal Stem Cells In Vivo. *Cell Stem Cell* 2017; **20**: 345–59.

81 Jansson D, Rustenhoven J, Feng S, Hurley D, Oldfield RL, Bergin PS, Mee EW, Faull RL, Dragunow M. A role for human brain pericytes in neuroinflammation. *J Neuroinflammation* 2014; **11**: 104.

82 Olson LE, Soriano P. PDGFRbeta Signaling Regulates Mural Cell Plasticity and Inhibits Fat Development. *Dev Cell* 2011; **20**: 815–26.

83 Jackson S, ElAli A, Virgintino D, Gilbert MR. Blood-brain barrier pericyte importance in malignant gliomas: what we can learn from stroke and Alzheimer's disease. *Neuro Oncol* 2017; **19**: 1173–82.

84 Enge M, Bjarnegård M, Gerhardt H, Gustafsson E, Kalén M, Asker N, Hammes HP, Shani M, Fässler R, Betsholtz C. Endothelium-specific platelet-derived growth factor-B ablation mimics diabetic retinopathy. *The EMBO Journal* 2002; **21**: 4307–16.

85 Winkler EA, Bell RD, Zlokovic BV. Central nervous system pericytes in health and disease. *Nat Neurosci* 2011; **14**: 1398–405.

86 Attwell D, Buchan AM, Charpak S, Lauritzen M, Macvicar BA, Newman EA. Glial and neuronal control of brain blood flow. *Nature* 2010; **468**: 232–43.

87 Fernández-Klett F, Priller J. Diverse functions of pericytes in cerebral blood flow regulation and ischemia. *J Cereb Blood Flow Metab* 2015; **35**: 883–7.

88 Yemisci M, Gursoy-Ozdemir Y, Vural A, Can A, Topalkara K, Dalkara T. Pericyte contraction induced by oxidative-nitrative stress impairs capillary reflow despite successful opening of an occluded cerebral artery. *Nat Med* 2009; **15**: 1031–7.

89 Hill RA, Tong L, Yuan P, Murikinati S, Gupta S, Grutzendler J. Regional blood flow in the normal and ischemic brain is controlled by arteriolar smooth muscle cell contractility and not by capillary pericytes. *Neuron* 2015; **87**: 95–110.

90 Armulik A, Genové G, Mäe M, Nisancioglu MH, Wallgard E, Niaudet C, He L, Norlin J, Lindblom P, Strittmatter K, Johansson BR, Betsholtz C. Pericytes regulate the blood-brain barrier. *Nature* 2010; **468**: 557–61.

91 Sagare AP, Bell RD, Zhao Z, Ma Q, Winkler EA, Ramanathan A, Zlokovic BV. Pericyte loss influences Alzheimer-like neurodegeneration in mice. *Nat Commun* 2013; **4**: 2932.

92 Kisler K, Nelson AR, Rege SV, Ramanathan A, Wang Y, Ahuja A, Lazic D, Tsai PS, Zhao Z, Zhou Y, Boas DA, Sakadžić S, Zlokovic BV. Pericyte degeneration leads to neurovascular uncoupling and limits oxygen supply to brain. *Nat Neurosci* 2017; **20**: 406–16.

93 De Jong GI, Farkas E, Stienstra CM, Plass JR, Keijser JN, de la Torre JC, Luiten PG. Cerebral hypoperfusion yields capillary damage in the hippocampal CA1 area that correlates with spatial memory impairment. *Neuroscience* 1999; **91**: 203–10.

94 Duncombe J, Lennen RJ, Jansen MA, Marshall I, Wardlaw JM, Horsburgh K. Ageing causes prominent neurovascular dysfunction associated with loss of astrocytic contacts and gliosis. *Neuropathol Appl Neurobiol* 2016; **43**: 477–91.

95 Wisniewski HM, Wegiel J, Wang KC, Lach B. Ultrastructural studies of the cells forming amyloid in the cortical vessel wall in Alzheimer's disease. *Acta Neuropathol* 1992; **84**: 117–27.

96 Szpak GM, Lewandowska E, Wierzba-Bobrowicz T, Bertrand E, Pasennik E, Mendel T, Stepień T, Leszczyńska A, Rafałowska J. Small cerebral vessel disease in familial amyloid and non-amyloid angiopathies: FAD-PS-1 (P117L) mutation and CADASIL. Immunohistochemical and ultrastructural studies. *Folia Neuropathol* 2007; **45**: 192–204.

97 Farkas E, De Jong GI, de Vos RAI, Jansen Steur ENH, Luiten PGM. Pathological features of cerebral cortical capillaries are doubled in Alzheimer's disease and Parkinson's disease. *Acta Neuropathol* 2000; **100**: 395–402.

98 Schultz N, Byman E, Fex M, Wennström M. Amylin alters human brain pericyte viability and NG2 expression. *J Cereb Blood Flow Metab* 2017; **37**: 1470–82.

99 Farkas E, Luiten PG. Cerebral microvascular pathology in aging and Alzheimer's disease. *Prog Neurobiol* 2001; **64**: 575–611.

100 Stewart PA, Hayakawa K, Akers MA, Vinters HV. A Morphometric Study of the Blood-Brain Barrier in Alzheimer's Disease. *Lab Invest* 1992; **67**: 734–42.

101 Bonkowski D, Katyshev V, Balabanov RD, Borisov A, Dore-Duffy P. The CNS microvascular pericyte: pericyte-astrocyte crosstalk in the regulation of tissue survival. *Fluids Barriers CNS* 2011; **8**: 8.

102 van Deurs B. Observations on the blood-brain barrier in hypertensive rats, with particular reference to phagocytic pericytes. *J Ultrastruct Res* 1976; **56**: 65–77.

103 Sengillo JD, Winkler EA, Walker CT, Sullivan JS, Johnson M, Zlokovic BV. Deficiency in mural vascular cells coincides with blood-brain barrier disruption in Alzheimer's disease. *Brain Pathol* 2013; **23**: 303–10.

104 Goodwin PC, Johnson B, Frevert CW. Chapter 4. Microscopy, Immuno-Histochemistry, Digital Imaging, and Quantitative Microscopy. In: Treuting PM, Dintzis SM, Montine KS, eds. Comparative Anatomy and Histology. San Diego, CA, USA: Elsevier Inc., 2017.

105 Grotta JC, Albers GW, Broderick JP, Kasner SE, Lo EH, Mendelow AD, Sacco RL, Wong LKS. Stroke: Pathophysiology, Diagnosis, and Management, 6th edn. Amsterdam, Netherlands: Elsevier Inc., 2016.

106 Mirra SS, Heyman A, McKeel D, Sumi SM, Crain BJ, Brownlee LM, Vogel FS, Hughes JP, van Belle G, Berg L. The Consortium to Establish a Registry for Alzheimer's Disease (CERAD). Part II. Standardization of the neuropathologic assessment of Alzheimer's disease. *Neurology* 1991; **41**: 479–86.

107 Fernández-Klett F, Brandt L, Fernández Zapata C, Abuelnor B, Middeldorp J, Sluijs JA, Curtis M, Faull R, Harris LW, Bahn S, Hol EM, Priller J. Denser brain capillary network with preserved pericytes in Alzheimer's disease. *Brain Pathol* 2020; **30**: 1071–86.

108 West MJ. Basic Stereology for Biologists and Neuroscientists. Cold Spring Harbor, NY, USA: Cold Spring Harbor Laboratory Press, 2012.

109 West MJ, Slomianka L, Gundersen HJG. Unbiased Stereological Estimation of the Total Number of Neurons in the Subdivisions of the Rat Hippocampus Using the Optical Fractionator. *Anat Rec* 1991; **231**: 482–97.

110 Mouton PR, Gokhale AM, Ward NL, West MJ. Stereological length estimation using spherical probes. *J Microsc* 2002; **206**: 54–64.

111 Keuker JIH, Vollmann-Honsdorf GK, Fuchs E. How to Use the Optical Fractionator: an Example Based on the Estimation of Neurons in the Hippocampal CA1 and CA3 Regions of Tree Shrews. *Brain Res Protoc* 2001; **7**: 211–21.

112 Schmitz C, Hof PR. Recommendations for straightforward and rigorous methods of counting neurons based on a computer simulation approach. *J Chem Neuroanat* 2000; **20**: 93–114.

113 Schmitz C, Hof PR. Chapter 4: Design-Based Stereology in Brain Aging Research. In: Riddle DR, ed. Brain Aging Models, Methods, and Mechanisms. Boca Raton, FL, USA: CRC Press., 2007.

114 Kreczmanski P, Heinsen H, Mantua V, Woltersdorf F, Masson T, Ulfig N, Schmidt-Kastner R, Korr H, Steinbusch HWM, Hof PR, Schmitz C. Microvessel length density, total length, and length per neuron in five subcortical regions in schizophrenia. *Acta Neuropathol* 2009; **117**: 409–21.

115 Flaherty JT, Pierce JE, Ferrans VJ, Patel DJ, Tucker WK, Fry DL. Endothelial Nuclear Patterns in the Canine Arterial Tree with Particular Reference to Hemodynamic Events. *Circ Res* 1972; **30**: 23–33.

116 Howard CV, Reed MG. Unbiased Stereology: Three-Dimensional Measurement in Microscopy, 1st edn. New York City, NY, USA: Springer, 1998.

117 Mann HB, Whitney D. On a test of whether one of two random variables is stochastically larger than the other. *The Annals of Mathematical Statistics* 1948; **18**: 50–60.

118 Lehmann EL. Nonparametrics: Statistical Methods Based on Ranks, revised 1st edn. New York City, NY, USA: Springer, 2006.

119 Kotz S, Read CB, Balakrishnan N, Vidakovic B, Johnson NL. Encyclopedia of statistical sciences, 2nd edn. Hoboken, NJ, USA: John Wiley & Sons, 2006.

120 American Psychological Association. Publication manual of the American Psychological Association, 6th edn. Washington, DC, USA: American Psychological Association, 2010.

121 Braak H, Braak E. Neuropathological stageing of Alzheimer-related changes. *Acta Neuropathol* 1991; **82**: 239–59.

122 Hardy J, Selkoe DJ. The amyloid hypothesis of Alzheimer's disease: progress and problems on the road to therapeutics. *Science* 2002; **297**: 353–6.

123 Sachdev PS, Zhuang L, Braidy N, Wen W. Is Alzheimer's a disease of the white matter? *Curr Opin Psychiatry* 2013; **26**: 244–51.

124 Ji F, Pasternak O, Ng KK, Chong JSX, Liu S, Zhang L, Shim HY, Loke YM, Tan BY, Venketasubramanian N, Chen CLH, Zhou JH. White matter microstructural abnormalities and default network degeneration are associated with early memory deficit in Alzheimer's disease continuum. *Sci Rep* 2019; **9**: 4749.

125 Brunnström HR, Englund EM. Cause of death in patients with dementia disorders. *Eur J Neurol* 2009; **16**: 488–92.

126 Sagare AP, Sweeney MD, Makshanoff J, Zlokovic BV. Shedding of soluble platelet-derived growth factor receptor-β from human brain pericytes. *Neurosci Lett* 2015; **607**: 97–101.

127 Miners JS, Schulz I, Love S. Differing associations between Aβ accumulation, hypoperfusion, blood-brain barrier dysfunction and loss of PDGFRB pericyte marker in the precuneus and parietal white matter in Alzheimer's disease. *J Cereb Blood Flow Metab* 2017; **38**: 103–15.

128 Li J, Hsu H-C, Mountz JD, Allen JG. Unmasking Fucosylation: from Cell Adhesion to Immune System Regulation and Diseases. *Cell Chemical Biology* 2018; **25**: 499–512.

129 Grammas P. Neurovascular dysfunction, inflammation and endothelial activation: Implications for the pathogenesis of Alzheimer's disease. *J Neuroinflammation* 2011; **8**: 26.

130 Nortley R, Korte N, Izquierdo P, Hirunpattarasilp C, Mishra A, Jaunmuktane Z, Kyrargyri V, Pfeiffer T, Khennouf L, Madry C, Gong H, Richard-Loendt A, Huang W, Saito T, Saido TC, Brandner S, Sethi H, Attwell D. Amyloid β oligomers constrict human capillaries in Alzheimer's disease via signaling to pericytes. *Science* 2019; **365**: eaav9518.

131 Rustenhoven J, Jansson D, Smyth LC, Dragunow M. Brain Pericytes As Mediators of Neuroinflammation. *Trends in Pharmacological Sciences* 2017; **38**: 291–304.

132 Vanlandewijck M, He L, Mäe MA, Andrae J, Ando K, Del Gaudio F, Nahar K, Lebouvier T, Laviña B, Gouveia L, Sun Y, Raschperger E, Räsänen M, Zarb Y, Mochizuki N, Keller A, Lendahl U, Betsholtz C. A molecular atlas of cell types and zonation in the brain vasculature. *Nature* 2018; **554**: 475–80.

133 Bell MA, Ball MJ. The Correlation of Vascular Capacity with the Parenchymal Lesions of Alzheimers-Disease. *Can J Neurol Sci* 1986; **13**: 456–61.

134 Goddard JC, Sutton CD, Furness PN, Kockelbergh RC, O'Byrne KJ. A computer image analysis system for microvessel density measurement in solid tumours. *Angiogenesis* 2002; **5**: 15–20.

135 Pogue AI, Lukiw WJ. Angiogenic signaling in Alzheimer's disease. *Neuroreport* 2004; **15**: 1507–10.

136 Bennett RE, Robbins AB, Hu M, Cao X, Betensky RA, Clark T, Das S, Hyman BT. Tau induces blood vessel abnormalities and angiogenesis-related gene expression in P301L transgenic mice and human Alzheimer's disease. *Proc Natl Acad Sci U S A* 2018; **115**: E1289–98.

137 Chakraborty A, Kamermans A, van het Hof B, Castricum K, Aanhane E, van Horssen J, Thijssen VL, Scheltens P, Teunissen CE, Fontijn RD, van der Flier WM, de Vries HE. Angiopoietin like-4 as a novel vascular mediator in capillary cerebral amyloid angiopathy. *Brain* 2018; **141**: 3377–88.

138 Tarkowski E, Issa R, Sjögren M, Wallin A, Blennow K, Tarkowski A, Kumar P. Increased intrathecal levels of the angiogenic factors VEGF and TGF-beta in Alzheimer's disease and vascular dementia. *Neurobiol Aging* 2002; **23**: 237–43.

139 Grammas P, Samany PG, Thirumangalakudi L. Thrombin and inflammatory proteins are elevated in Alzheimer's disease microvessels: Implications for disease pathogenesis. *J Alzheimers Dis* 2006; **9**: 51–8.

140 Thirumangalakudi L, Samany PG, Owoso A, Wiskar B, Grammas P. Angiogenic proteins are expressed by brain blood vessels in Alzheimer's disease. *J Alzheimers Dis* 2006; **10**: 111–8.

141 Masliah E, Mallory M, Alford M, Deteresa R, Saitoh T. PDGF is associated with neuronal and glial alterations of Alzheimer's disease. *NBA* 1995; **16**: 549–56.

142 Provia J, Jeynes B. Reduction in Vascular Endothelial Growth Factor Expression in the Superior Temporal, Hippocampal, and Brainstem Regions in Alzheimer's Disease. *Curr Neurovasc Res* 2014; **11**: 202–9.

143 Yang S-P, Bae D-G, Kang HJ, Gwag BJ, Gho YS, Chae C-B. Co-accumulation of vascular endothelial growth factor with beta-amyloid in the brain of patients with Alzheimer's disease. *NBA* 2004; **25**: 283–90.

144 Cunvong K, Huffmire D, Ethell DW, Cameron DJ. Amyloid-β Increases Capillary Bed Density in the Adult Zebrafish Retina. *Invest Ophthalmol Vis Sci* 2013; **54**: 1516–21.

145 Cameron DJ, Galvin C, Alkam T, Sidhu H, Ellison J, Luna S, Ethell DW. Alzheimer's-related peptide amyloid-β plays a conserved role in angiogenesis. *PLoS ONE* 2012; **7**: e39598.

146 Grammas P, Tripathy D, Sanchez A, Yin X, Luo J. Brain microvasculature and hypoxia-related proteins in Alzheimer's disease. *Int J Clin Exp Pathol* 2011; **4**: 616–27.

147 Grammas P, Martinez J, Sanchez A, Yin X, Riley J, Gay D, Desobry K, Tripathy D, Luo J, Evola M, Young A. A new paradigm for the treatment of Alzheimer's disease: targeting vascular activation. *J Alzheimers Dis* 2014; **40**: 619–30.

148 Singh C, Pfeifer CG, Jefferies WA. Pathogenic Angiogenic Mechanisms in Alzheimer's Disease. In: Simionescu D, Simionescu A, eds. Physiologic and Pathologic Angiogenesis - Signaling Mechanisms and Targeted Therapy. Rijeka, Croatia: InTech, 2017.

149 Althouse AD. Adjust for Multiple Comparisons? It's Not That Simple. *Ann Thorac Surg* 2016; **101**: 1644–5.

150 Little RJ, D'Agostino R, Cohen ML, Dickersin K, Emerson SS, Farrar JT, Frangakis C, Hogan JW, Molenberghs G, Murphy SA, Neaton JD, Rotnitzky A, Scharfstein D, Shih WJ, Siegel JP, Stern H. The Prevention and Treatment of Missing Data in Clinical Trials. *N Engl J Med* 2012; **367**: 1355–60.

Eidesstattliche Versicherung

Ich, Lasse Brandt, versichere an Eides statt durch meine eigenhändige Unterschrift, dass ich die vorgelegte Dissertation mit dem Thema: „Pericytes in Alzheimer's Disease: A Morphometric Analysis“ selbstständig und ohne nicht offengelegte Hilfe Dritter verfasst und keine anderen als die angegebenen Quellen und Hilfsmittel genutzt habe.

Alle Stellen, die wörtlich oder dem Sinne nach auf Publikationen oder Vorträgen anderer Autoren beruhen, sind als solche in korrekter Zitierung (siehe „Uniform Requirements for Manuscripts (URM)“ des ICMJE – *www.**icmje**.org*) kenntlich gemacht. Die Abschnitte zu Methodik (insbesondere praktische Arbeiten, Laborbestimmungen und statistische Aufarbeitung) und Resultaten (insbesondere Abbildungen, Grafiken und Tabellen) entsprechen den URM (s.o.) und werden von mir verantwortet.

Meine Anteile an etwaigen Publikationen zu dieser Dissertation entsprechen denen, die in der untenstehenden gemeinsamen Erklärung mit dem Betreuer, angegeben sind. Sämtliche Publikationen, die aus dieser Dissertation hervorgegangen sind und bei denen ich Autor bin, entsprechen den URM (s.o.) und werden von mir verantwortet.

Die Bedeutung dieser eidesstattlichen Versicherung und die strafrechtlichen Folgen einer unwahren eidesstattlichen Versicherung (§156,161 des Strafgesetzbuches) sind mir bekannt und bewusst.

Datum Unterschrift

Anteilserklärung an etwaigen erfolgten Publikationen

Lasse Brandt hatte folgenden Anteil an den folgenden Publikationen:

Publikation 1 (Poster; XI European Meeting on Glial Cells in Health and Disease, Berlin, 3.-6. Juli 2013):

Brandt L*, Fernández-Klett F*, Harris LW, Bahn S, Priller J. Pericytes are preserved in Alzheimer's disease. *Glia* 2013; **61**: 65–6. doi:10.1002/glia.22530. *Contributed equally as co–first authors.

Publikation 1 beinhaltet vorläufige Anteile des Abstracts, der Einleitung, der Methoden, der Ergebnisse und der Diskussion dieser Dissertation.

Lasse Brandt, Dr. Francisco Fernández-Klett und Prof. Dr. Josef Priller sind verantwortlich für Konzept und Design des Projekts sowie für die Interpretation der Daten. Lasse Brandt führte alle im Methodenteil beschriebenen Schritte durch und wertete die Ergebnisse aus. Lasse Brandt ist verantwortlich für das Abstract, die Einleitung, die Methoden, die Resultate und die Diskussion. Die Supervision und Korrektur der Publikation 1 erfolgte durch Dr. Francisco Fernández-Klett und Prof. Dr. Josef Priller.

Publikation 2 (Artikel):

Fernández-Klett F*, Brandt L*, Fernández Zapata C, Abuelnor B, Middeldorp J, Sluijs JA, Curtis M, Faull R, Harris LW, Bahn S, Hol EM, Priller J. Denser brain capillary network with preserved pericytes in Alzheimer's disease. *Brain Pathol* 2020; **30**: 1071–86. doi:10.1111/bpa.12897. *Contributed equally as co–first authors.

Publikation 2 beinhaltet Anteile des Abstracts, der Einleitung, der Methoden, der Ergebnisse und der Diskussion dieser Dissertation. Die Abbildungen 1-4 und Tabelle 1 dieser Dissertation sind adaptiert aus Publikation 2.

Dr. Francisco Fernández-Klett, Lasse Brandt und Prof. Dr. Josef Priller sind verantwortlich für Konzept und Design des Projekts sowie für die Interpretation der Daten. Lasse Brandt führte die stereologische Analyse und alle darauf bezogenen Schritte im Methodenteil durch. Lasse Brandt war nicht beteiligt an der Clearing-Analyse und der Genotypisierung. Dr. Francisco Fernández-Klett, Lasse Brandt und Prof. Dr. Josef Priller erstellten das Manuskript für die Publikation 2.

_____

Unterschrift, Datum und Stempel des betreuenden Hochschullehrers

_____

Unterschrift des Doktoranden

Mein Lebenslauf wird aus datenschutzrechtlichen Gründen in der elektronischen Version meiner Arbeit nicht veröffentlicht.

Mein Lebenslauf wird aus datenschutzrechtlichen Gründen in der elektronischen Version meiner Arbeit nicht veröffentlicht.

Mein Lebenslauf wird aus datenschutzrechtlichen Gründen in der elektronischen Version meiner Arbeit nicht veröffentlicht.

Acknowledgements

Foremost, I sincerely thank Prof. Dr. Josef Priller, who gave me the opportunity to pursue my research under his supervision. His guidance and advice were of great value to me.

I am very grateful to Dr. Francisco Fernández-Klett for his inspiration, encouragement, and support in this project.

I wish to thank the members of the Laboratory of Molecular Psychiatry at Campus Charité Mitte, including post doctorate researchers, doctorate students, and technical assistants as well as cooperation partners. In particular, I would like to thank PD Dr. Chotima Böttcher, Dr. Jojanneke Huck, Dr. Mihovil Mladinov, Christian Böttcher, and Jasmin Jamal El-Din for the very helpful discussions.

Dr. Ingo Przesdzing provided great insights into stereological methods and I thank him for his advice.

I am thankful for the stipend (SFB/TRR 43) and the grant that supported the project (SFB/TRR167) by the German Research Foundation.

I would like to express my gratitude for my family for their love and support.